DEVELOPMENT OF MECHANICALLY ROBUST, BIODEGRADABLE BIOINK FORMULATIONS FOR 3D BIOPRINTING

A THESIS SUBMITTED TO
THE GRADUATE SCHOOL OF NATURAL AND APPLIED SCIENCES
OF
ANKARA UNIVERSITY

by

Işıl YAZGAN

IN PARTIAL FULFILLMENT OF THE REQUIREMENTS
FOR THE DEGREE OF
MASTER OF SCIENCE
IN
BIOMEDICAL ENGINEERING

ANKARA
2023

ABSTRACT

M.Sc. Thesis

DEVELOPMENT OF MECHANICALLY ROBUST, BIODEGRADABLE BIOINK FORMULATIONS FOR 3D BIOPRINTING

Işıl YAZGAN

Ankara University
Graduate School of Natural and Applied Sciences
Department of Biomedical Engineering

Supervisor: Prof. Dr. Pınar YILGÖR HURİ

Clinical cases including trauma and long-term denervation could cause volumetric skeletal muscle loss that necessitate surgical repair since the tissue has limited ability of self-repair and the regenerated tissue is generally co-observed with fibrosis leading to poor functional and mechanical properties. Along with scarcity of the donor tissue available for transplantation in the surgical treatments, they are generally accompanied by significant donor site morbidity. As a result of these shortcomings, engineering functional skeletal muscle tissue via tissue engineering technique holds great promise for the remediation of the aforementioned clinical cases. One of the application areas of this technique is 3D printing. The production of living tissue substitutes is possible with 3D bioprinting that makes use of the bioinks. However, there are some current limitations of the technique, such as the unavailability of an ideal bioink material with suitable rheological, mechanical and elastic properties that match that of skeletal muscle. Therefore, there is a need for the development of novel biomaterials with suitable mechanical properties that can mimic the structure and function of skeletal muscle tissue. Polyurethanes (PU) are biomaterials composed of "soft" and "hard" segments. With the appropriate design and selection of hard and soft segments, it is possible to obtain PUs with desired properties.

In this thesis, PU-based, light-curable novel bioink materials were developed. Structural and mechanical characterization of the novel materials were performed, along with assessment of 3D printability and stability after cross-linking. Moreover, cytotoxicity assessment and in vitro analysis with C2C12 mouse myoblasts were performed. Among the plethora of PUs synthesized, methacrylated polyurethane (PUMA)-6 was found to be suitable as a light-curable, biocompatible and biodegradable bioink material.

July 2023, 76 pages

Key Words: Tissue Engineering; 3D Bioprinting; Bioink; Polyurethane; Skeletal Muscle

ÖZET

Yüksek Lisans Tezi

3B BİYOBASKI İÇİN MEKANİK STABİLİTEYE SAHİP, BİYOBOZUNUR BİYOMÜREKKEP FORMÜLASYONLARININ GELİŞTİRİLMESİ

Işıl YAZGAN

Ankara Üniversitesi
Fen Bilimleri Enstitüsü
Biyomedikal Mühendisliği Anabilim Dalı

Danışman: Prof. Dr. Pınar YILGÖR HURİ

Travma ve uzun süreli denervasyon dahil olmak üzere klinik vakalar, dokunun sınırlı kendi kendini tamir etme kabiliyetine sahip olması ve rejenere dokunun genellikle zayıf fonksiyonel ve mekanik özelliklere yol açan fibroz ile birlikte gözlenmesi nedeniyle cerrahi onarım gerektiren hacimsel iskelet kası kaybına neden olabilmektedir. Cerrahi tedavilerde, transplantasyona uygun donör dokunun azlığı yanında genellikle önemli donör saha morbiditesi de eşlik etmektedir. Bu eksikliklerin bir sonucu olarak, doku mühendisliği tekniği ile fonksiyonel iskelet kası dokusunun mühendisliği, yukarıda belirtilen klinik vakaların iyileştirilmesi için büyük umut vaat etmektedir. Bu tekniğin genişleyen uygulama alanlarından biri de kişiye özel ve anatomik olarak doğru yapılar üretme potansiyeline sahip 3B baskıdır. Biyomürekkeplerden yararlanan 3B biyobaskı ile canlı doku ikamelerinin üretimi mümkündür. Ancak uygun hücre-malzeme etkileşimlerinin yanı sıra iskelet kası yapısına uygun reolojik, mekanik ve elastik özelliklere sahip ideal bir biyomürekkep malzemesi bulunmamaktadır. Bu nedenle, 3B biyobaskıda kullanılmak üzere iskelet kası dokusunun yapısını ve işlevini taklit edebilen, uygun mekanik özelliklere sahip ve biyouyumlu biyomalzemelerin geliştirilmesine ihtiyaç vardır. Poliüretanlar (PU), makromoleküler bir omurga boyunca kimyasal olarak bağlanmış "yumuşak" ve "sert" segmentlerden oluşan biyomalzemelerdir. Sert ve yumuşak segmentlerin uygun tasarımı ve seçimi ile istenen özelliklere sahip PU'lar elde etmek mümkündür.

Bu tezde, PU bazlı, ışıkla kürlenebilen özgün biyomürekkep malzemeleri geliştirilmiştir. Bunların yapısal ve mekanik karakterizasyonu, 3B basılabilirlik ve çapraz bağlamadan sonra stabilite değerlendirmesi gerçekleştirilmiştir. Ayrıca, sitotoksisite değerlendirmesi ve C2C12 fare miyoblastları ile in vitro analiz gerçekleştirilmiştir. Sentezlenen birçok PU arasında, metakrilatlanmış poliüretan (PUMA)-6'nın ışıkla çapraz bağlanan, biyolojik olarak uyumlu ve biyobozunur bir biyomürekkep malzemesi olarak uygun olduğu belirlenmiştir.

Temmuz 2023, 76 sayfa

Anahtar Kelimeler: Doku Mühendisliği; 3B Biyobaskı; Biyomürekkep; Poliüretan; İskelet Kası

FOREWORD AND ACKNOWLEDGEMENTS

I would like to present my heartfelt gratitude and respect to my precious supervisor Prof. Dr. Pınar YILGÖR HURİ, who guided me with her invaluable knowledge and experience during the two years I furthered my master's degree and provided me with all of the opportunities for my thesis studies. I appreciate the compassion and time she devoted to me during this period.

I wish to express my endless appreciation and respect to Prof. Dr. İskender YILGÖR, Emel YILGÖR, and Dr. İpek ATAY (Koç University) for the information they conveyed about the synthesis of polyurethane, the main material of my thesis, the interest they showed to me and the infrastructure opportunities they provided for me during my thesis studies.

I would also would like to thank Prof. Dr. Hikmet ALTUNAY and Prof. Dr. Alp CAN for giving me the opportunity to perform and analyze the cell staining data.

I am deeply thankful to my lab mentors Dr. Emre ERGENE and Şeyda GÖKYER, who always provided me with their vast knowledge and experience throughout my laboratory studies, guided me and supported me in the problems I encountered. I would also like to express my gratitude to my colleagues Barış ALTUNAY, Osama Ali ALHİNDY, Utku Serhat DERİCİ and Ayşe YALÇINER for their unwavering support during all my studies.

This thesis was carried out within the scope of the TÜBİTAK Center of Excellence Support Program (1004 Program) directed by Ankara University Stem Cell Institute (Project no: 20AG003), within the Project-5 titled “3D Bioprinting and Biomimetic Stimulation for Engineering Functional Skeletal Muscle Tissue”. I am thankful for the financial support provided through this project.

I am very grateful to the Ankara University Department of Biomedical Engineering for the opportunities they provided during the course of my education, and to the Musculoskeletal Tissue Engineering Laboratory, where I carried out all my studies.

I would like to express my gratitude to my dear friend A. Kaan ÖZMEN, who did not leave me alone in this adventure, never spared his unconditional support, and stood by me in all my weal and woe.

Finally, I would like to thank my lovely mother and father, who have always stood behind me all my life and whose financial and moral support I have always felt, and my brother Serhat and sister Sena, who have always been by my side.

Işıl YAZGAN
Ankara, July 2023

TABLE OF CONTENTS

ABBREVIATIONS

2D	Two-Dimensional
3D	Three-Dimensional
Alg	Alginate
AM	Additive manufacturing
ASCs	Adipose-derived stem cells
ATP	Adenosine triphosphate
BSA	Bovine serum albumin
C2C12	Mouse myoblast cell line
$CaCl_2$	Calcium chloride
CAD	Computer-aided design
CT	Computed tomography
dECM	Decellularized extracellular matrices
DMEM	Dulbecco's Modified Eagle Medium
DMSO	Dimethyl Sulfoxide
ECM	Extracellular Matrix
ESCs	Embryonic stem cells
EY	Eosin Y
FBS	Fetal bovine serum
FDM	Fused deposition modeling
FGF-2	Fibroblast growth factor-2
FTIR	Fourier Transform Infrared Spectroscopy
GelMA	Gelatin Methacrylate
HDI	Hexamethylene diisocyanate
IPA	Isopropyl alcohol
iPSCs	Induced pluripotent stem cells
L929	Mouse fibroblast cell line
MA	Maleic anhydride
MAA	Methacrylic anhydride
MRI	Magnetic resonance imaging

PCL	Poly(ε-Caprolactone)
PEO	Poly(ethylene oxide)
PFA	Paraformaldehyde
PGA	Polyglycolic Acid
PHEMA	Polyhydroxyethyl methacrylate
PI	Photoinitiator
PLA	Polylactic Acid
PLGA	Poly(lactic-co-glycolic acid)
P/S	Penicillin streptomycin
PU	Polyurethane
PUMA	Polyurethane-maleic anhydride
PUMAA	Polyurethane-methacrylic anhydride
PUs	Polyurethanes
SLA	Stereolithography
SLM	Selective laser melting
SLS	Selective laser sintering
TEA	Triethanolamine
THF	Tetrahydrofuran
USD	United States dollar
UV	Ultraviolet
VP	1-vinyl-2- pyrrolidone

LIST OF FIGURES

LIST OF TABLES

1. INTRODUCTION

Skeletal muscle has the potential to regenerate after an injury, but its regeneration potential is limited in cases of large-volume muscle loss. Since there is no effective drug therapy that triggers muscle recovery and the amount of autologous muscle flaps that can be used is insufficient, functional skeletal muscle conjugates are needed in the treatment. Conditions such as genetic diseases, post-traumatic defects, aggressive tumor ablation and long-term denervation often represent clinical conditions that cause volumetric muscle loss and require surgical reconstruction by transferring healthy donor muscle tissue into the defect (Schaefer et al., 2020). This is accompanied by significant donor site morbidity. Damaged soft tissue, especially skeletal muscle, has insufficient ability to self-repair, and the regenerated tissue shows low mechanical and functional properties. Therefore, the generation of skeletal muscle tissue using tissue engineering techniques holds promise for the treatment of the clinical challenges mentioned above (Li et al., 2007; Liao & Zhou, 2009). Engineered three-dimensional (3D) skeletal muscle tissue constructs can restore both function as well as the contour of the defect area.

Tissue engineering is an interdisciplinary field that applies the principles of engineering and life sciences to the development of biological substitutes that repair, restore and/or improve tissue function (Langer, 2000). Recent research has greatly increased awareness of the dramatic differences in cell behavior between two-dimensional (2D) and 3D culture systems. Culturing cells in 3D provides a more physiologically favorable environment to guide cell behavior and enhance their function (Puschmann et al., 2013; Thoma et al., 2014). Therefore, 3D biofabrication techniques that can create complex and functional 3D architectures with appropriate biomaterials and cells to mimic the natural microenvironment and biological components are used in tissue engineering (Zhu et al., 2016).

In large-volume muscle loss, there are limitations on the functional regeneration of skeletal muscle tissue (MacLean et al., 2012). The tissue engineering method aims to find a solution to this global health problem with the production of functional skeletal

muscle in the laboratory environment and to produce an effective solution for use in muscle regeneration. There are studies in the literature on the production of skeletal muscle by 3D bioprinting (Merceron et al., 2015; Choi et al., 2016; García-Lizarribar et al., 2018). However, these studies have some limitations. Materials frequently used for 3D printing are hydrogel-like materials such as decellularized extracellular matrix (ECM)-based bioink (Choi et al., 2016) or gelatin methacrylate (GelMA) (García-Lizarribar et al., 2018), but the mechanical properties required for active muscle contraction are not met by these materials. Moreover, the required durability, elasticity and recovery upon stretch are also typically not met with these materials. Although biomaterials such as poly(ε-caprolactone) (PCL) have the appropriate mechanical strength and properties, they are not suitable for providing the structural and biological features of natural tissue such as low stiffness, and proper cell-material interactions. Therefore, there is a need for the development of biocompatible, biodegradable, unique biomaterials with suitable mechanical properties that can mimic the structure and function of skeletal muscle tissue for use in 3D bioprinting applications.

Polyurethanes (PUs) are polymeric materials that are widely used as biomaterials since they can be synthesized in a wide variety of chemical structures and properties (Yilgor et al., 2015). PUs are an important class of polymers that can be obtained with thermoplastic or elastomeric properties due to their physicochemical properties (Ergene et al., 2019a). Since the versatile polyurethane chemistry allows for the development of very different polymers in terms of chemical, structural and mechanical properties; polyurethane (PU)-based biomaterials can be synthesized with appropriate strength and elasticity that can mimic that of the skeletal muscle. Because of these favorable properties, PUs can be used in the production of scaffolds for soft tissues, including skeletal muscle (Vannozzi et al., 2017). In addition to the favorable structural and mechanical properties, preparation of PU in the form of a cell-laden hydrogel, also known as the “bioink” will reveal unique opportunities for 3D bioprinting applications. Development of such bioinks with favorable structural, mechanical and biocompatible features are highly required in the literature.

Within the scope of this thesis, the development of PU-based bioink with unique features

including biocompatibility, hydrogel features and elastomeric properties required for 3D bioprinting of elastic and actively load-bearing tissues such as skeletal muscle, suitable for use with a 3D bioprinter system is discussed. It is aimed to use the novel PU-based biomaterials as photocurable bioink materials for skeletal muscle tissue engineering. Unlike other studies available in the literature in the field of skeletal muscle tissue engineering with 3D printing, in this study, the homogeneous distribution of cells in mechanically suitable tissue scaffolds was achieved by using PU-based bioink. Synthesis, characterization and investigation of cell-material interactions were performed. A patent application was filed based on the findings of this thesis study.

2. LITERATURE SURVEY

2.1 Skeletal Muscle

There are about 700 muscles in the human body with different functions that undertake very important tasks. These muscles are classified as cardiac muscle, smooth muscle and skeletal muscle that undertake various functions such as circulation, movement and heat production. Skeletal muscles make up about 50% of body weight and contain about 75% of body proteins (Frontera & Ochala, 2015). They provide the movement as well as helping to maintain the energy balance (Rivas & Fielding, 2013). Skeletal muscle tissue is sensitive to nutrition, movement, physical activities and prone to injury and several diseases. Decrease in muscle mass creates deficiency in the immune system, since skeletal muscles are depots for many organs, especially the brain and the heart (Wolfe, 2006). Due to all these important functions for the body, prevention of muscle mass loss, strengthening of the muscle, seeking solutions to muscle diseases, re-functioning the muscles that cannot be repaired by building muscle-like structures are among the important research topics of today.

2.1.1 Structure of skeletal muscle

Skeletal muscles consist of parallel aligned myofibers (muscle fibers) with multinucleated structure. Each of these nuclei is responsible for a protein synthesized in that region (S. Hikida, 2011). Skeletal muscles contain connective tissues known as perimysium that surround myofibers, neural networks, and blood vessels. These connective tissues are surrounded by another connective tissue called epimysium. Satellite cells in the myofibers between the sarcolemma and the basal lamina are adult stem cells that are responsible for muscle growth and regeneration (Macaluso & Myburgh, 2012). Skeletal muscles composed of striated, parallel aligned and densely packed bundles of myofibers (McCullen et al., 2009), and myofibrils are composed of sarcomeres, the basic contractile unit. Sarcomeres are formed by the hexagonal arrangement of the two main motor proteins, actin and myosin filaments (**Figure 2.1**).

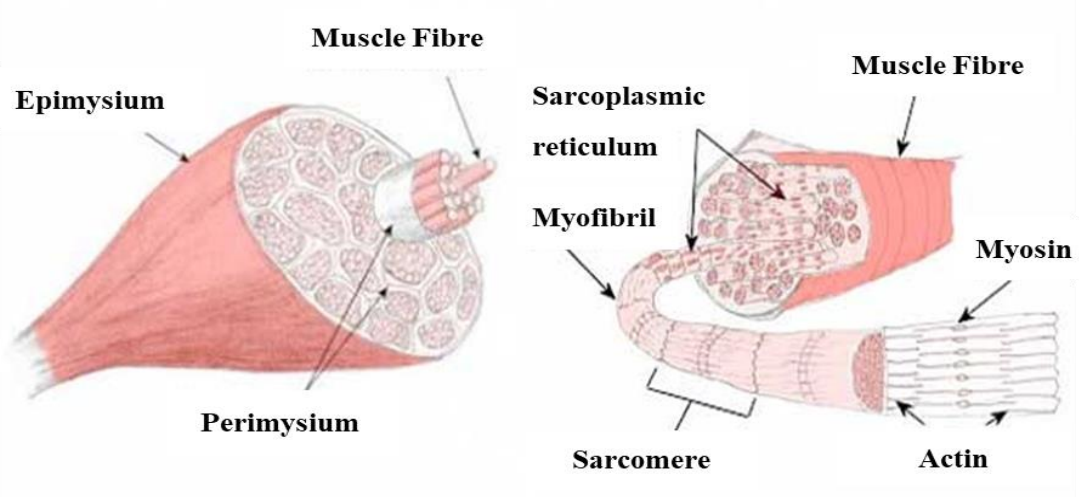

Figure 2.1 Structure of skeletal muscle (Michael Walden, 2022)

Actin and myosin filaments play an important role in cell movement. Actin is a round-shaped and structural protein. It polymerizes in a helical shape to form actin filaments, also known as microfilaments. Actin filaments form the cellular skeleton and provide mechanical support to the cell, determine the shape of the cell, and allow the cell to move. In muscle cells, together with the protein called myosin, they take a role in the formation of the contraction action. Myosins are thick filaments of protein structure that interact with actin filaments in muscle cells and provide contraction. Myosins are a family of adenosine triphosphate (ATP)-dependent motor proteins. Muscle cells contain "myosin II" and make up 55% of the total muscle protein mass. It regulates the contraction and relaxation movements of the muscles by forming actomyosin together with actin. Muscle contraction and relaxation is explained by the sliding of actin and myosin filaments over each other (Cooper GM, 2000).

2.1.2 Clinical approaches for the regeneration of skeletal muscle

Skeletal muscle, which is one of the largest tissues that makes up about half of the body weight, is frequently damaged by various reasons such as high-energy trauma, tumor removal, congenital or acquired diseases such as Duchenne Muscular Dystrophy, and unconscious sports activities (Huard et al., 2002). Although muscle tissue has the ability to regenerate when adult stem cells (satellite cells) in its structure are activated as a

result of damage, it is known that this mechanism cannot be completed and functional muscle recovery does not occur in large volume losses (MacLean et al., 2012). In such cases, a worldwide health expenditure of 6 billion United States Dollars (USD) is made every year to ensure muscle regeneration (Quintero et al., 2009). An effective solution has not yet been found for the treatment of large-volume muscle defects, which constitute a large part of these health expenditures.

The treatment method used in the clinic in cases of massive muscle losses is the transplantation of autologous free muscle flaps to the damaged area. Reasons such as the insufficient amount of autologous muscle flaps that can be used and the fact that synthetic materials that will act as a muscle have not been developed yet bring about new searches for the acquisition of functional muscle tissue (Turner & Badylak, 2012). The tissue engineering method aims to find a solution to this global health problem with the production of functional skeletal muscle in the laboratory environment and to produce an effective solution for use in muscle regeneration. There are studies in the literature on the production of skeletal muscle by 3D bioprinting (Merceron et al., 2015; Choi et al., 2016; García-Lizarribar et al., 2018). However, these studies have some limitations. Most of the materials used for 3D printing are hydrogel materials and cannot provide sufficient mechanical strength. Biomaterials such as PCL, on the other hand, are not suitable for providing properties such as elasticity, although they have mechanical strength. Therefore, there is a need to develop biocompatible, biodegradable, unique biomaterials with suitable mechanical properties that can mimic the structure and function of skeletal muscle tissue for use in 3D bioprinting applications.

2.2 Tissue Engineering

Tissues or organs are frequently damaged and lose their functionality due to high-energy traumas such as traffic accidents, congenital anomalies, cancer or sports injuries. In such cases where treatments are inadequate, tissue and organ transplantation are the first choice to reconstruct damaged tissues and organ (Ikada, 2006). However, donor

shortage has led to the research and application of other methods. One of the most important of these methods is the use and attention of tissue engineering as an alternative approach for tissue and organ reconstruction (Han et al., 2020; Moysidou et al., 2021). Tissue engineering is an interdisciplinary field of research that aims to repair and regenerate missing or damaged tissues with a combination of carrier scaffolds made of biocompatible materials and cells and growth factor agents (Shafiee & Atala, 2017).

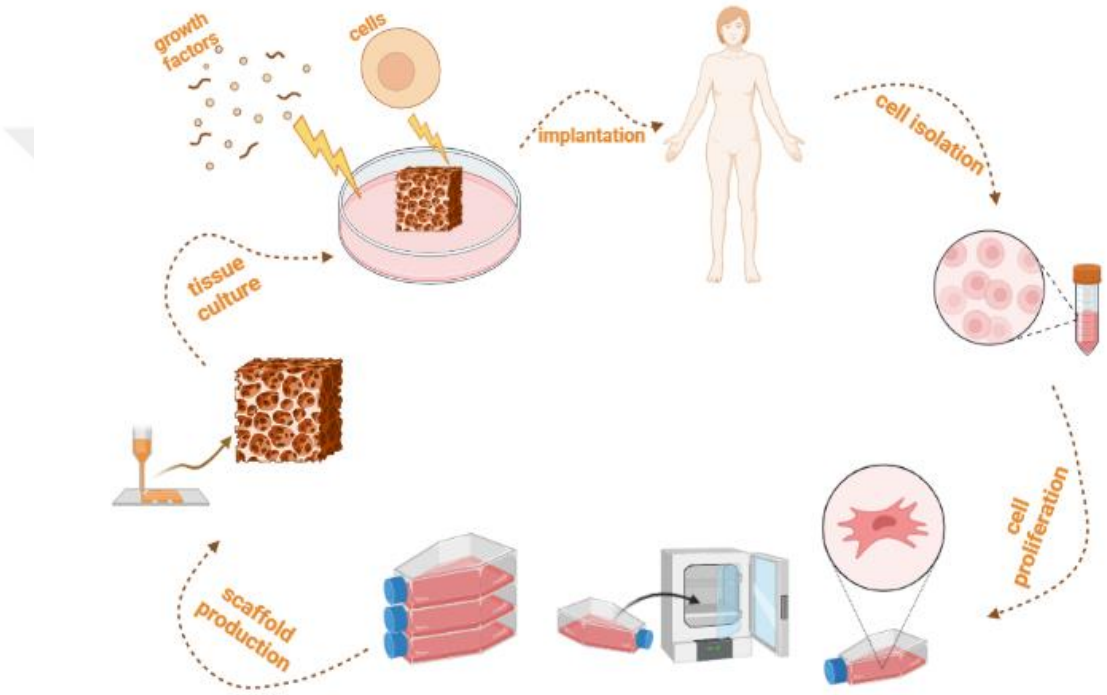

Figure 2.2 Tissue engineering workflow (Designed with Biorender.)

The process applied in tissue engineering approach is given schematically in **Figure 2.2**. This process is generally examined in five parts. Cells obtained from the patient with appropriate cell selection is the first step of this process. In addition to the use of cells completely isolated from the patient's own tissues, various cell lines or specialized cells such as induced pluripotent stem cells (iPSCs) can be used as needed. In the next step, the isolated cells are propagated in the appropriate culture medium to reach a sufficient amount. At the same time, the scaffolds that will carry these cells are usually produced by 3D printers using natural biodegradable polymers, synthetic polymers or

decellularized extracellular matrices (dECM). These scaffolds can be produced with or without cells as appropriate. In the following stage, the carrier scaffold is taken into the tissue culture medium together with the cells and growth factors, and the cell-material interaction is completed. At the last stage, the tissue culture is completed and the mature carrier scaffold is transferred to the damaged area and the process is completed (Langer & Vacanti, 1993; Qazi et al., 2015).

The selection of the cell source, which is the first step in tissue engineering processes, is very important and it is generally preferred to use primary cells from the healthy region of the target tissue isolated from the patient. Problems arise from, time to time, in the isolation and reproduction of these cells in the laboratory. For this reason, the use of stem cells as a cell source has an important place in tissue engineering. Stem cells are the cells that make up the structure of tissues and organs in the body. They can renew themselves and differentiate into other cells. There are three main types: Embryonic stem cells (ESCs), IPSCs and adult stem cells. Transcription factors such as Oct4, Sox2 Klf4 and cMyc are given to the somatic cell and these cells are transformed into pluripotent cells. This is defined as IPSC and in this way the cell is reprogrammed (Friedmann-Morvinski & Verma, 2014). In addition to the selection of the cell source, the selection of scaffolds is another important element of tissue engineering. Therefore, 3D biofabrication techniques that can create complex, functional 3D architectures with appropriate biomaterials and cell types to mimic the natural microenvironment and biological components are used in tissue engineering (Zhu et al., 2016).

2.2.1 Skeletal muscle tissue engineering

Skeletal muscle tissue engineering and regeneration is a subfield that is studied, researched and questioned in tissue engineering applications. Interest in this field is increasing day by day. Skeletal muscle tissue engineering aims to construct muscle tissues in vitro using the strategies of implanting damaged tissue or replacing scar tissue. In the regeneration approach used for therapeutic purposes in skeletal musculoskeletal disorders, it is aimed to develop tissue-like scaffolds that can be implanted for the

formation of new muscle from the tissue remaining in vivo to the damaged area (Gokyer et al., 2021).

Scaffolds are preferred to ensure the function and survival of the cells used and to create mechanical stability (Cezar & Mooney, 2015). The biocompatibility of the material is one of the important issues in the production of scaffolds. Fibrinogen, alginate, collagen and hyaluronic acid used as materials are natural polymers, but their mechanical properties are not good. Materials such as PCL, poly(lactic-co-glycolic acid) (PLGA) are synthetic materials and although their strength is higher, their biocompatibility is lower. For this reason, the search for new materials continues and combinations of natural and synthetic materials continue to be tried (Ergene et al., 2019b). The cytotoxicity problems encountered in synthetic polymers and their low interaction with the cell have led to hydrogel-based materials. Hydrogels are water-swellable, cross-linked polymeric structures. They can be prepared in different shapes and forms, they can be obtained from natural or synthetic polymers, and they can be sterilized by heat. They have different application areas such as contact lenses, artificial tendon material, artificial skin and artificial muscle (Wang et al., 2020). In one of the studies conducted in skeletal muscle tissue engineering applications, myoblasts were isolated and injected into the relevant region. This procedure was unsuccessful and cell death has been reported after injection (Fan et al., 1996). Since other studies using stem cells could not obtain positive results, it was emphasized that it would not be possible to treat large volumes of muscle loss with cells alone, and the need for the production of scaffolds that support that area. In order for these scaffolds to mimic muscle tissue, it is important that they have appropriate mechanical stability, be suitable for 3D printing, and be biodegradable (Winkler et al., 2011). In this direction, it has been reported that myotube formation has increased in studies using scaffolds (Kim et al., 2018; Ku et al., 2012).

2.2.2 Scaffolds for skeletal muscle tissue engineering

Biomaterials used in scaffold designs are the basic building blocks of tissue engineering applications. Scaffolds created using biomaterials must be biocompatible,

biodegradable, with appropriate mechanical properties, porous and 3D structure. Natural and synthetic polymers are generally used as biomaterials in tissue engineering (Pati et al., 2015; Khademhosseini & Langer, 2016). Although natural polymers have advantages in terms of biocompatibility, the mechanical stability of synthetic polymers and their ability to be designed as desired make these materials stand out.

Table 2.1 Biomaterials frequently used in skeletal muscle tissue engineering

Natural Polymers	Synthetic Polymers
Hyaluronic Acid	Poly(ε-Caprolactone)
Chitosan	Polylactic Acid (PLA)
Alginate	Polyglycolic Acid (PGA)
Gelatin	Silicon
Collagen	Polyethylene Glycol
Elastin	Polyurethane

Natural polymers are naturally occurring biopolymers that can be obtained in nature from animals, plants, fungi, etc. Since they are formed naturally, their biocompatibility is high, their toxic effects are low, they are biodegradable and easily accessible. Although they have these advantages, they are structurally complex and extraction processes are long and expensive (Muhamad et al., 2014). Due to such shortcomings, synthetic polymers have also been frequently used.

Synthetic polymers are readily available and manufacturing processes are faster. Their lower cost compared to natural polymers is another reason for preference. It is important for tissue engineering that they are biocompatible and can show mechanical stability suitable for the targeted tissue. However, their toxic effects are higher compared to natural polymers (Muhamad et al., 2014).

Table 2.1 lists several natural and synthetic polymers frequently used in skeletal muscle tissue engineering. Protein-based polymers such as collagen and gelatin, and others such as alginate and chitosan are abundant in nature. Collagen and gelatin provide superior

properties for cell-material interactions since they are the natural components of the extracellular matrix of most of the tissues (Malafaya et al., 2007). Materials such as alginate and chitosan are also frequently preferred due to their high biocompatibility as well as suitable stability and mechanical properties (Cascone et al., 2001). Among the synthetic polymers, PCL, PLA, PGA are the most preferred material types in tissue engineering. Although they are preferred due to their mechanical strength, durability, stability and cost as well as being suitable for 3D printing due to their thermoplastic behavior, they have limitations including stiffness mismatch especially with the soft tissues. Moreover, they are not suited for use as bioinks.

2.2.2.1 Polyurethane

Polyurethanes (PU) are among the most important polymers used as biomaterials. There are a large number of monomers available, and therefore there is a great versatility for many different types of polymer design and synthesis (Yilgor et al., 2015). They are especially suited for use in engineering of soft and elastic tissues like skeletal muscle and vessels due to their favorable durability, elasticity and other mechanical properties.

PUs consist of alternating "soft" and "hard" segments that are chemically linked along a macromolecular backbone (**Figure 2.3**). With the appropriate design, selection and chemical combination of hard and soft segments, it is possible to obtain PUs with desired flexibility, mechanical strength and various other surface and volume properties (Yilgor et al., 2015). The ratios of these soft and hard parts in the polymer, their chemical structures determine the physical and chemical properties of PUs. While materials such as PCL and poly(ethylene glycol) (PEG) are generally preferred for the soft segments, diisocyanates are used for the hard segments.

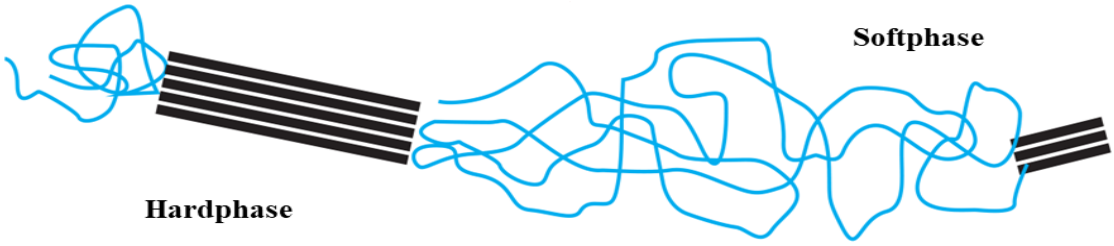

Figure 2.3 PU copolymers with soft and hard segments (Koslen, 2020)

There are very few examples in the literature on the use of PUs as bioink material. In a study, PU was used as a bioink for nerve tissue engineering (Ho & Hsu, 2018). It was reported that the degradation of the material synthesized is not suited for the intended use. Therefore, PUs are generally preferred in studies that require a graft material with extended degradation times within the body.

2.2.3 Scaffold production techniques

It is important that scaffolds are biocompatible, biodegradable, easily sterilized, easily produced, have sufficient mechanical stability, have suitable chemical properties and be porous in order to facilitate the proliferation of cells by providing nutrient and oxygen transfer. To provide these features, various production techniques have been developed (Tuzlakoglu et al., 2005). One of them is the phase separation technique, and in this technique, materials with two separate phases are used in order to obtain porous structures. The solvent group is removed from the materials and reduced to a single phase. Generally, porous structures ranging between 20 and 200 µm can be obtained. In the freeze-drying method, it is generally aimed to produce porous structures in the presence of acetic acid. Under vacuum, the frozen material is expected to crystallize and form pores. The method of producing scaffolds without using solvents to prevent the toxic effects of organic solvents is known as gas foaming. Foaming is done using polymers and carbon dioxide. The porosity size usually has a value of 100 µm (Can & Ersoy, 2014). In spinning methods, filaments are formed by passing the liquid polymer through the spinneret. If the polymer is in a molten state and does not break down in this phase, a filament is obtained by the melt spinning method. In this method, the molten polymer is passed through the spinnerets and cooled, resulting in filament formation.

The formation of filaments by dissolving the polymer in a solvent and passing it through spinnerets is called solution spinning. In solution spinning, if the solvent is removed with hot air or steam, it is called dry spinning. If solidification is achieved in the presence of a coagulation bath, it is called wet spinning (Kramschuster & Turng, 2013). However, scaffold design and reproducibility with the desired properties are quite difficult in these techniques.

Additive manufacturing (AM) methods have an increasing importance and application field in tissue engineering. The technique is based on assembling and combining individual parts together in a layer-by-layer manner for the production of any 3D product. 3D models are made into 3D products with this technique at a rapid pace, as well as providing high freedom of design and production.

2.2.3.1 3D printing

3D printing, commonly referred to as additive manufacturing or rapid prototyping, is the process of making computer-generated digital models into actual physical products. 3D design softwares, medical imaging data or 3D surface scans can provide the 3D models required. 3D printing technique is used in various different industrial fields including aerospace and defense, architecture as well as medicine (Dawood et al., 2015). The first applications of 3D printing in medicine was in the 1990s (Strub et al., 2006). Particularly, preliminary research has been done on the production of custom craniofacial implants.

Medical 3D printing operations typically start with the identification of the patient's anatomy and/or the defect site, and medical imaging data generated with X-ray, computed tomography (CT) or magnetic resonance imaging (MRI) (Aimar et al., 2019). The segmentation procedure then labels the generated images. The aim of this procedure is to isolate the desired area and create a 3D model in the computer. Computer-aided design (CAD) software is one of the most crucial components for 3D printing, especially given the growth of the technology (Miyazaki & Hotta, 2011). The appropriate designs

are created for 3D object development with the aid of CAD programs. To enable printing on printers, the 3D model is converted to STL file after it has been created (Satyanarayana & Prakash, 2015). Although it varies depending on the type of printer, in general, the printing of the file begins after the set of the parameters, such as print speed and pressure, and the pertinent optimization processes are carried out. As a result, customized 3D objects are created based patient's data (**Figure 2.4**).

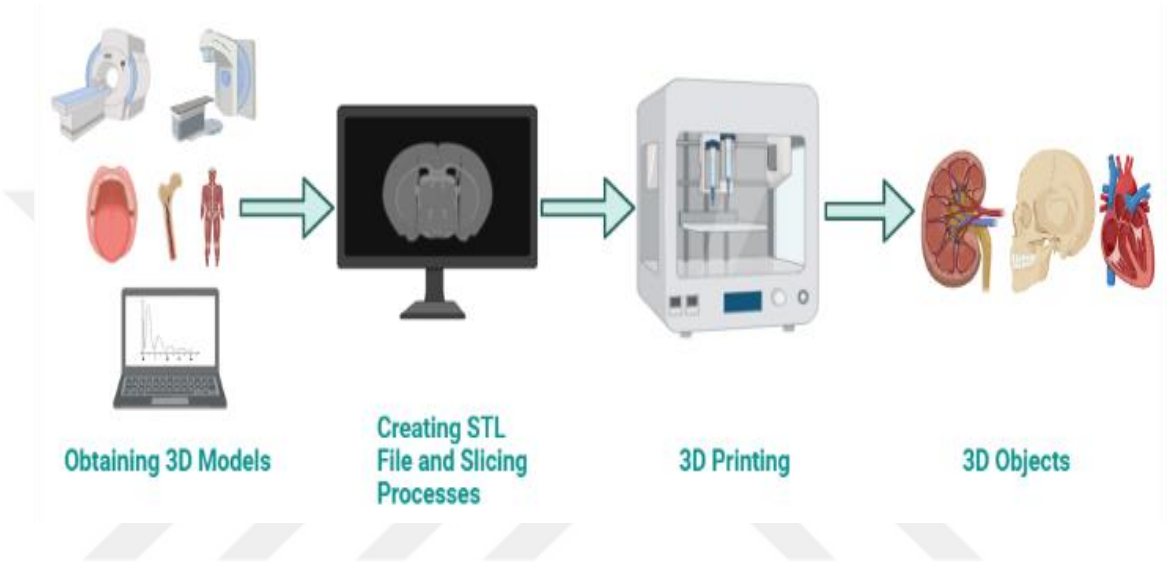

Figure 2.4 3D printing process (Designed with Biorender)

Since the advent of 3D printers, a variety of production methods have been developed, including stereolithography (SLA), fused deposition modeling (FDM), selective laser sintering (SLS), and selective laser melting (SLM) (H. J. Chen, 2012). Depending on how it is utilized in the medical area, the printing substance used, and the printing time needed, each method has different benefits and drawbacks.

Cardiology, urology, orthopedics, plastic surgery, and gastroenterology are just a few of the professions that use 3D printing, which is a rapidly evolving technology in the medical field (Aimar et al., 2019). Making customized designs, selecting the materials to be utilized, and processing images from patients in various geometries are steps followed in medical 3D printing (Dawood et al., 2015).

2.2.3.2 Bioprinting

Bioprinting is the process of 3D printing of the living cells within biomaterials that are commonly referred to as “bioinks” (Derby, 2012). It is possible to create living, functional tissues and organs in the laboratory environment by bioprinting (Murphy & Atala, 2014a). Accordingly, the distinction between the terms 3D printing and 3D bioprinting is that 3D printing of cell-laden biomaterials take place in 3D bioprinting as opposed to 3D printing, which does not use biological structures for printing (**Figure 2.5**) (Vijayavenkataraman et al., 2018).

Similar to 3D printing, 3D models are developed in a computer environment using imaging techniques like X-ray, CT, and MRI. Design strategies like biomimicry and self-assembly are also available (Murphy & Atala, 2014b). Inkjet, extrusion, and laser bioprinting are the three main technologies utilized for bioprinting after the design phase is completed. The substance that is connected to cells is flowing in the form of droplets during inkjet bioprinting. According to the computer-generated models, they gather at the intended location. Drops demonstrate flow at the specified pressure and speed (Xu et al., 2008). Complex structures can be created more easily using this method of printing because droplet modifications are possible. When using extrusion bioprinting, filaments are used. Since there is a constant flow of filaments, fluid materials must be used. According to Melchels et al., 2012, the deposited structure must be robust and have a low solubility in comparison to the others. A laser beam, a ribbon, and a film holding ingredients are needed for laser bioprinting. The films are situated on the ribbon, which is where the laser is absorbed. Because there is no spraying involved with laser bioprinting, there is no clogging. Due to the application of laser radiation, cell viability is less than that of other types (Xia et al., 2018).

There are additional requirements for the materials used in bioprinting since the substance must be 3D printable, and mechanically durable while also being compatible with biological components. This subject is constrained by the lack of material diversity in this regard. Bioprinting involves the use of materials like alginate, chitosan,

polyethylene glycol, and gelatin. The choice of the proper cells is another aspect that is equally crucial to the materials. If the cell proliferation rate is very low, then functional tissue regeneration is generally not obtained. If there is uncontrolled cell proliferation, it generally induces apoptotic pathways. In this direction, several different cell types including the mesenchymal stem cells are frequently used for 3D bioprinting (Murphy & Atala, 2014a).

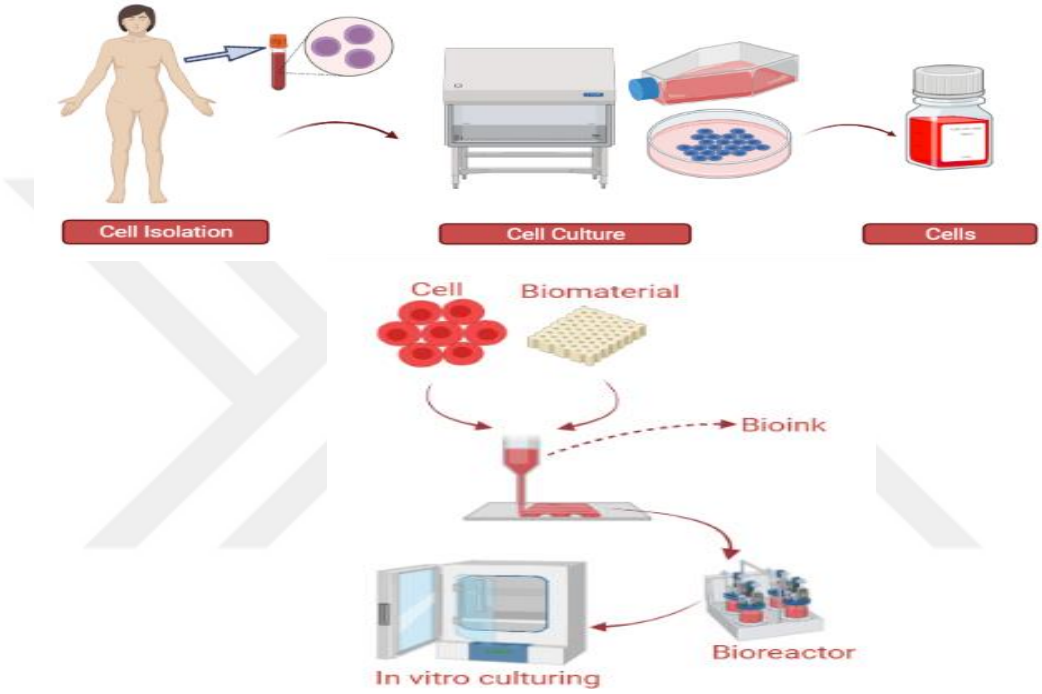

Figure 2.5 Demonstration of bioprinting process (Designed with Biorender)

Aortic valve (Hockaday et al., 2012), human skin (Lee et al., 2014), bionic ear (Mannoor et al., 2013), neural structures (XU et al., 2006), and blood vessel-like structures (Skardal et al., 2010) are just a few of the tissue and organ studies that have been generated by bioprinting. Although bioprinting shows promise, the selection of materials needs to be broadened. The printers utilized should have better performance metrics like speed and resolution. In addition, there is a need for many different studies focusing on the production of functional and durable tissues and organs.

2.2.3.3 Bioinks

Hydrogels are three-dimensional hydrophilic polymer networks that can swell by holding a large portion of water (Ferreira et al., 2018). They are known for their insolubility in water. Hydrogels are frequently preferred in tissue engineering since they resemble the structure of the extracellular matrix (Radhakrishnan et al., 2014). There are many hydrogels available, both of natural and synthetic origin. The history of contact lenses produced with cross-linked polyhydroxyethyl methacrylate (pHEMA), among the first hydrogel applications in the medical field, dates back to the 1960s (WICHTERLE & LÍM, 1960). Hydrogels are generally classified according to their crosslinking properties, preparation methods and sources. They are divided into physical or chemical cross-linking according to their cross-linking patterns. Looking at the preparation methods, homopolymers are obtained from a single monomer species. Copolymers consist of two or more monomers arranged randomly in chains of polymer networks. According to their sources, hydrogels are divided into natural and synthetic. Collagen, alginate, acrylic acid, methacrylic acid can be given as the main examples (Ullah et al., 2015).

Hydrogels are typically obtained by the combination of monomers/polymers, photoinitiators and crosslinkers (Ahmed, 2015a). Their cross-linking can be achieved via curing with ultraviolet (UV) light, visible light and even by heat. In **Figure 2.6**, polymer formation from monomers and hydrogel production from these polymers with the aid of crosslinkers are simulated.

Figure 2.6 Hydrogel formation (Designed with Biorender)

Hydrogels can respond to stimuli such as temperature, pH, light, and therefore have many different uses. Because of the high biocompatibility of hydrogels, a negative interaction is not frequently encountered when integrated into the body. For this reason, they are commonly preferred as biomaterials (ULUSOY & DİKMEN, 2020). They are used as wound dressings, drug delivery, contact lenses, and tissue engineering applications (Caló & Khutoryanskiy, 2015). As a dressing, hydrogels can absorb toxins, retain moisture, and prevent overheating. In drug transport, it has been reported that after the drug is added to the monomer and polymerized, it is trapped in the hydrogel and thus transported (Peppas, 2000). A soft and moist environment is important when using contact lenses. Hydrogels have a structure that provides both this environment and oxygen permeability (Lloyd et al., 2001). Due to all these mentioned features, its importance in medicine is increasing day by day.

Bioinks are obtained by adding cells to hydrogel materials to be 3D printed (AKKUŞ et al., 2020). Cells are combined with the material, resulting in cell-laden scaffolds after printing. The main purpose here is that the cells take the shape of the desired tissue and degrade the material. The ability to mimic tissue, high cell-cell interactions, short and easy bioprinting steps are among the most important advantages (Hospodiuk et al., 2017).

It is important to choose the appropriate bioinks according to the tissue being studied. Mechanical, biological, rheological and physical properties are the factors that should be considered in the selection of bioinks. These properties also affect cell growth, printability, tissue healing, and biocompatibility (Gungor-Ozkerim et al., 2018). Examples of biomaterials that can be used in bioinks are polymers and hydrogels. Hydrogels are ideal for cell encapsulation as they can swell without dissolving in an aqueous medium (Ahmed, 2015b). In addition, they are preferred because they have high cell adhesion and adjustable mechanical properties (Lei & Wang, 2016). The main polymers used as bioink are chitosan, alginate, collagen, fibrin and gelatin methacrylate (Akkuş et al., 2020).

Duration of the bioprinting times depend on the size and porosity of the design to be printed. When decellularized matrices and hydrogels are compared, it has been reported that hydrogels take a shorter time to bioprint, but tissue formation time is faster in matrices (Yin Yu & Ozbolat, 2014).

Moreover, there are many challenges in the use of bioinks. Reducing cell loss, improving mechanical properties, and vascularizing tissue structures are subjects that need to be studied. Hydrogels, which are the most preferred group as bioink, limit the interactions of cells as they form a physical barrier by encapsulating the cells. When the concentrations are increased, their mechanical strength increases, but cell viability decreases. They degrade more slowly in cell culture media and toxicity problems may occur (Hospodiuk et al., 2017). Considering all these problems, it will be inevitable to produce, design and develop new bioprintable materials in the future.

2.3 Scope and Novelty of The Study

This thesis aimed to develop novel PU-based bioink materials that have proper biocompatibility, biodegradability and elastomeric properties which are required for 3D bioprinting of elastic and actively load-bearing tissues such as skeletal muscle. Synthesis, characterization and cytotoxicity assessment of novel PU-based bioink materials were performed. Moreover, investigation of the interactions of these materials with the skeletal myoblast cells were performed in in vitro conditions. In this study, different types of PU-based, light-curable polymers with high specificity were synthesized in collaboration with project partners at Koç University Department of Chemistry (in the scope of AU 1004 Project 20AG003). Chemical, mechanical and cytotoxicity analysis were carried out with a plethora of novel PU-based materials. Methacrylated PU (PUMA)-6 was used as a bioink using mouse myoblast cell line (C2C12), and scaffolds were bioprinted to investigate cell-material interactions; namely, sprouting and proliferation of the cells within the bioink matrix under in vitro conditions. As a result, PU-based elastomeric bioink materials were developed within the context of this thesis study for the first time in the literature, which are highly required for the 3D bioprinting of actively functioning soft tissues such as the skeletal muscle.

3. MATERIALS AND METHODS

3.1 Materials

The materials used within the scope of this thesis and their intended use are presented in **Table 3.1**.

Table 3.1 The materials used, their suppliers and intended use within this thesis

Material	**Brand / Company**	**Intended Use**
L929 mouse fibroblast cell line	ATCC	Cytotoxicity test
C2C12 mouse myoblast cell line	ATCC	Cell-material interaction studies
Fetal bovine serum (FBS)	Biological Industries	Cell culture medium
Penicillin streptomycin (P/S)	Biological Industries	Cell culture medium
Dulbecco's Modified Eagle Medium (DMEM) (high glucose)	Biological Industries	Cell culture medium
Trypsin	Biological Industries	Detachment of adherent cells
Dimethyl Sulfoxide (DMSO)	Sigma-Aldrich	Cell freezing
Paraformaldehyde (PFA)	Merck	Fixation of samples
Alamar Blue	Thermo Fisher	Cell viability analysis
Alexa Fluor 488 Phalloidin	Thermo Fisher	Actin filament staining
DAPI	Thermo Fisher	Nuclei labeling
Live/Dead™ Kit	Thermo Fisher	Staining of live and dead cells

Table 3.1 The materials used, their suppliers and intended use within this thesis (continued)

Triton X100	Merck	Immunofluorescent staining
Bovine serum albumin (BSA)	Sigma-Aldrich	Immunofluorescent staining
Sodium alginate (medium viscosity)	Sigma-Aldrich	Scaffold production
GelMA	Sigma-Aldrich	Scaffold production
1-vinyl-2- pyrrolidone (VP)	Sigma-Aldrich	Photoinitiator
Eosin Y (EY)	Sigma-Aldrich	Photoinitiator
Triethanolamine (TEA)	Merck	Photoinitiator
Alginate lyase (10,000 unites/g)	Sigma-Aldrich	Scaffold production
Calcium chloride ($CaCl_2$)	Sigma-Aldrich	Crosslinking
Tetrahydrofuran (THF)	Merck	Solvent
Isopropyl alcohol (IPA)	Merck	Solvent

3.2 Methods

Various PU-based polymers were synthesized by Koç University Department of Chemistry, Polymer Research Laboratory to be used as bioinks. 3D printability and crosslinking properties of these polymers were investigated thoroughly before the onset of cell-based investigations.

3.2.1 Polyurethane-Maleic anhydride (PUMA) synthesis

Figure 3.1 represents the synthesis procedure of polyurethane-maleic anhydride (PUMA). Synthesis is based on the termination of amino end groups of 1,6-hexamethylene diisocyanate (HDI) which is urea linking group, and poly(ethylene oxide)

(PEO) based polyurea copolymers with maleic anhydride (MA). HDI and MA groups are in the hard group of the polymer, while PEO is in the soft group. **Figure 3.1** shows the synthesis processes of MA-terminated HDI-PEO-urea copolymers by following the two-step reaction method. As shown in **Figure 3.1**, in these polymers, codenamed PUMA-X, X indicates the average number of HDI-PEO urea groups in the chain.

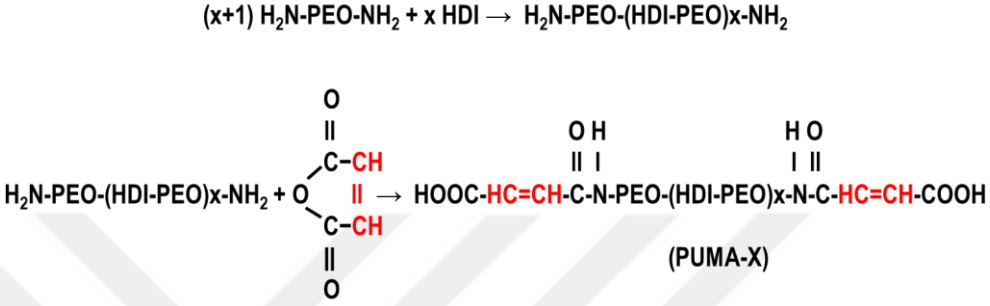

Figure 3.1 Schematic representation of PUMA synthesis

During the polymer synthesis, the number of X was determined as 2, 6 and 33 and 3 different polymers were synthesized accordingly. The average molecular weights of these materials are presented in **Table 3.2**.

Table 3.2 Chemical structure synthesized PUMA polymers

Code	X	Molecular Weight (g/mol)
PUMA-2	2	2,500
PUMA-6	6	6,000
PUMA-33	33	28,000

3.2.2 Polyurethane-Methacrylic anhydride (PUMAA) synthesis

10% (w/w) PU in tetrahydrofuran (THF)/isopropyl alcohol (IPA) (1:1) was added dropwise into a 1% (w/v) MAA. Following completion of the reaction, the solution was

poured into Teflon molds and solvent was evaporated for 24 h. The resulting polymer film was used for further investigations.

3.2.3 Polymer characterization

3.2.3.1 FTIR

FTIR analysis was performed to investigate the completion of PUMAA and PUMA synthesis. Reactions were monitored using the Nicolet 7600 FTIR spectrometer.

3.2.3.2 Measurement of viscosity

Polymer viscosity was characterized by using a Malvern Kinexus Rhemoeter. For this, the plate diameter was set as 25 mm and the gap between the plate and the sample was set as 500 µm. Measurements were made at a logarithmic ramp of 1^{-1000} s^{-1} and a temperature of 23°C. The shear rate is expressed as s^{-1} and the dynamic viscosity value is expressed as Pa.s.

Storage modulus (G') and loss modulus (G") of polymers were characterized by using a Malvern Kinexus Rhemoeter. For this, the plate diameter was set as 25 mm and the gap between the plate and the sample was set as 500 µm. Measurements were made at a temperature of 37°C. For the frequency sweep test of the polymers, the frequency was set at range of 0.1 to 100 Hz.

3.2.3.3 Mechanical characterization

Mechanical properties of the polymers were studied by a uniaxial tensile test on a Shimadzu mechanical tester (AGS – X). For this, each film is mounted on the clamps of the device with a 50 N load cell (**Figure 3.2**). The original length (L_0) and thickness were measured (L_0: 20 mm, cross-sectional area: 0.5 mm^2). Then, the tensile test was

started and the films were stretched at a rate of 5 mm/min at room temperature until the specimen had ruptured. Young's Modulus was calculated from the initial linear regions of the stress/strain curves.

Ultimate Tensile Strength (UTS) was reported as the maximum stress before rupture and the percent elongation at break (EOB) values were calculated using the length of the films prior to rupture and the initial length.

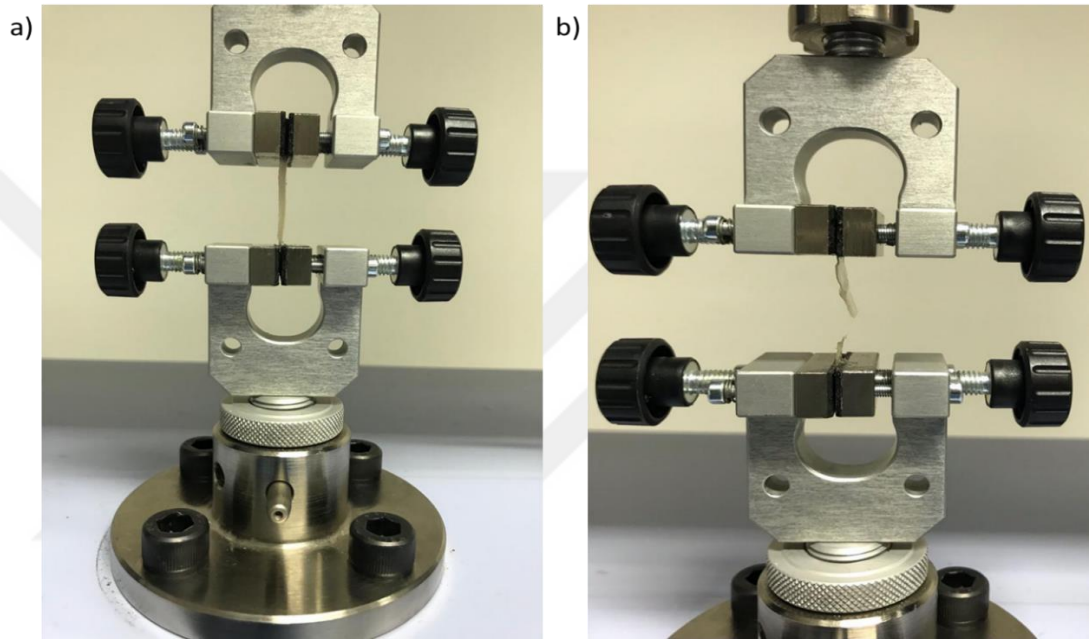

Figure 3.2 Application of uniaxial tensile test to the polymer films, a) before, and b) after the rupture of the sample

3.2.3.4 Scanning electron microscopy (SEM) analysis

The morphological features of the hydrogels (as well as the cell-laden bioinks) were evaluated by SEM. For this, the samples were lyophilized (cell-laden bioinks were fixed with formaldehyde prior to this step) and placed on carbon tapes adhered to SEM sample holders (stub). After the sputter coating with gold, the samples were observed with the Quanta 400F Field Emission SEM device of the METU Central Laboratory.

3.2.4 *in vitro* studies

3.2.4.1 Cytotoxicity assessment

In order to determine the cytotoxicity of the materials used, indirect cytotoxicity tests were carried out in accordance with the MEM-extraction test specified in 10993/EN 30993. Based on the microscopic data obtained in accordance with the cytotoxicity test, scoring is made according to the evaluation criteria given in **Table 3.3**. According to this table, the grades obtained from the first three criteria (spread of the cell layer, amount of dead cells and change in cell morphology) are averaged. This average grade is then added with the grade from the last criterion (cell growth inhibition) to obtain the final cytotoxic response index value, ranging from 0 to 8 as presented in **Table 3.4**. This value is used to evaluate whether the material is cytotoxic.

Table 3.3 Cytotoxicity test evaluation criteria

	Evaluation Criteria	**Grade**
Spread of The Cell Layer (Confluency)	100%	0
	90-100%	1
	60-90%	2
	30-60%	3
	0-30%	4
Amount of Dead Cells	Never seen	0
	0-5%	1
	5-10%	2
	10-20%	3
	≥ 20%	4

Table 3.3 Cytotoxicity test evaluation criteria (continued)

Change in Cell Morphology	No change observed	0
	Little change, few cells affected	1
	Moderate change, some cell morphology changed	2
	Moderate change, change in morphology of many cells	3
	High level of change, change in morphology of all cells observed	4
Cell Growth Inhibition	0-10%	0
	10-30%	1
	30-50%	2
	50-70%	3
	70-100%	4

Table 3.4 Cytotoxic response index and cytotoxicity assessment

Cytotoxic Response Index	**Reactivity**	**"Material is Cytotoxic"**
0-1	No	No
1-3	Little	No
3-5	Middle	should be reevaluated
5-7	More	Yes
7-8	A lot	Yes

Samples were sterilized by exposure to UV light (400 nm) for 30 min prior to the tests. UHMWPE was used as the positive control and Latex was used as a negative control since it was known to have a cytotoxic effect (Baek et al., 2005). Cell culture medium was used as the extraction fluid (10% FBS and 1% P/S in 89% high glucose DMEM). 12.5 mg of PUMA-2, PUMA-6 and PUMA-33 samples were added to 5 mL of extraction media and kept under continuous shaking at 60 rpm for 24 h in 15 mL falcon tubes.

L929 cells were transferred into T75 flasks in cell culture medium (10% FBS and 1% P/S in 89% high glucose DMEM). It was cultured in an incubator at standard culture conditions (37 ^{o}C, 5% CO_2 and humidity) for 24 h. Cells were seeded in 24-well cell culture dishes at a concentration of 5000 cells/cm^2. When the cells cultured under standard culture conditions in a CO_2 incubator for 24 hours became approximately 70% confluent, morphological evaluations were made with an inverted light microscope (Zeiss Primovert Inverted, Germany) and then the extraction liquids were added to the cell plates at 1000 µL/well.

Extraction liquids obtained from the samples were added to the cell monolayer in triplicates for each group. At 24 and 48 hours after the addition of the extraction liquids, the confluency of the cell layer and the changes in the cell morphology were evaluated by microscopic examination. The data obtained from the microscopic examination were compared with the positive and negative control groups and graded according to the evaluation criteria given in **Table 3.3**. Grades obtained from the first three criteria (spread of the cell layer, amount of dead cells and change in cell morphology) were averaged. This average grade was added to the grade obtained from the last criterion (cell growth inhibition) and used to obtain the final cytotoxic response index value ranging from 0 to 8 (**Table 3.4**). This value was used to evaluate whether the produced material was cytotoxic.

3.2.4.2 Cell culture

Cryopreserved C2C12 (CRL-1772, ATCC) cells were thawed by gentle pipetting within cell culture media and centrifuged to collect the pellet. Viable cells were counted via a hemocytometer by using trypan blue to distinguish the dead cells. Live cells remain as unstained under the light microscope. Cells were plated in T75 flasks at 5,000 cells/cm2 concentration. Flasks were incubated within the CO2 incubator under standard cell culture conditions (5% CO_2 and 37^{o}C). The medium within the flask was changed every other day until the cells were 80-90% confluent. Remaining cells were stored in a freezing solution containing 10% DMSO, 50% DMEM, and 40% FBS in a liquid

nitrogen tank until use.

3.2.4.3 Preparation of light-curable PU-based bioink

PUMA-2, PUMA-6 and PUMA-33 were used to develop light-curable bioinks. Photoinitiators were used to obtain efficient gelation by using blue (visible) and UV light.

In the study of Noshadi et al., 2017, three different components were used to obtain a bioink with GelMA. Firstly, Eosin Y was used as a photoinitiator and TEA was used as the co-initiator. VP used as a co-monomer is indicated as an accelerator of gelation. These materials can absorb light in the visible region (400-550 nm) (Annabi et al., 2014). In this system, when Eosin Y is exposed to visible light, it shifts from ground state to triplet state. This means the presence of unpaired electrons in the environment and extracts the hydrogen atoms of the TEA. The formed TEA radical begins to interact with methacryloyl groups. VP, which is used as an accelerator in this process, where gelation begins, is used to form a sufficient number of radicals (Lim et al., 2008). The effectiveness of Eosin Y in these interactions during the bioink formation stages given in **Figure 3.3** can also be visually determined by changing the color of the material from red to yellow. In these cross-linking reactions, the concentrations of Eosin Y, TEA and VP chemicals affect the cross-linking.

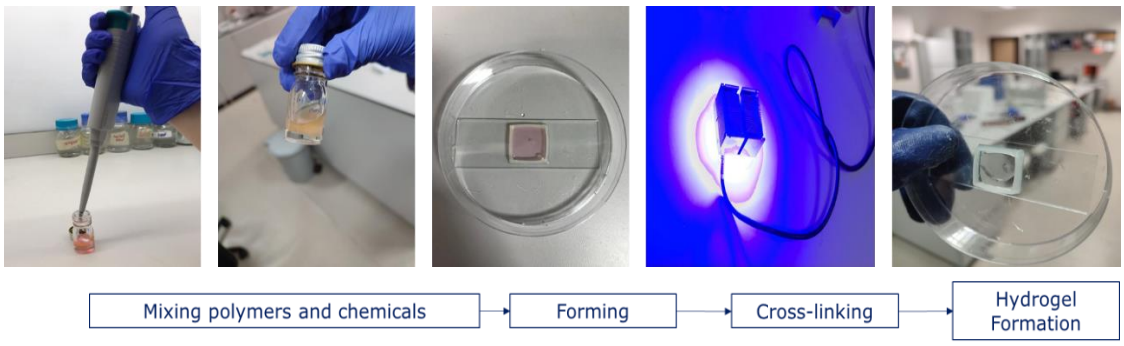

Figure 3.3 Preparation of PUMA gels under visible light

,

In the light of this information, PUMA hydrogel formation was optimized by studying the effect of the parameters given in **Table 3.5**. For this, PUMA-2, PUMA-6, PUMA-33 and/or their blends were added into distilled water. Then, TEA and VP were added into these solutions. Finally, Eosin Y was added and mixed overnight at room temperature at 500 rpm on a magnetic stirrer. Effect of polymer and photoinitiator concentrations on the printability as well as the crosslinking efficiency were investigated.

Table 3.5 Parameters optimized to obtain light curable PU-based hydrogel

Polymer Type	Polymer Concentration (w/v %)	Photoinitiator Concentration (v/v %)	Light Source	Crosslinking time (min)
PUMA-2	20-65	20-70	UV + Visible Light	5-10
PUMA-6	20-100	20-100	UV + Visible Light	5-20
PUMA-33	20-65	20-30	UV + Visible Light	5
PUMA-33-2 (Blend)	90	100	UV Light	10
PUMA-33-6 (Blend)	75-100	60-100	UV Light	10-20

3.2.4.4 Bioprinting

Cell culture studies were carried out to optimize bioink properties including viscosity (printability), gelling, cell adhesion/sprouting, cell proliferation and long-term stability of the constructs. These parameters are listed in **Table 3.6**. 3D bioprinting was performed at 37°C, 2.5 bar pressure, 8.5 mm/s print speed using Envisiontec 3D Bioprinter.

Table 3.6 Bioink parameters optimized to enhance printability, cellular viability and sprouting

Polymer Type	Polymer Concentration (w/v %)	Photoinitiator Concentration (v/v %)	Crosslinking time (min)	Cell Concentration (Cells / μL)
PUMA-6	75-90	60-100	10-20	2500
PUMA-33-6 (Blend, 50:50)	90-100	60-100	20	2500
PUMA-6-GelMA (Blend, 50:50)	30	30	3	2500
PUMA-6-GelMA-Alginate (Blend, 49:49:2)	31	30	5	2500

Figure 3.4 represents the steps followed during 3D bioprinting. First, polymer solutions were prepared within the photoinitiators under sterile conditions after sterilization by UV irradiation (400 nm wavelength; distance of 30 cm) for 30 minutes. Cells were resuspended in 100 μL of culture medium and added within the polymer matrix to obtain the bioink. 3D bioprinting was performed and photocrosslinking was done by UV light to ensure gelation of the printed products.

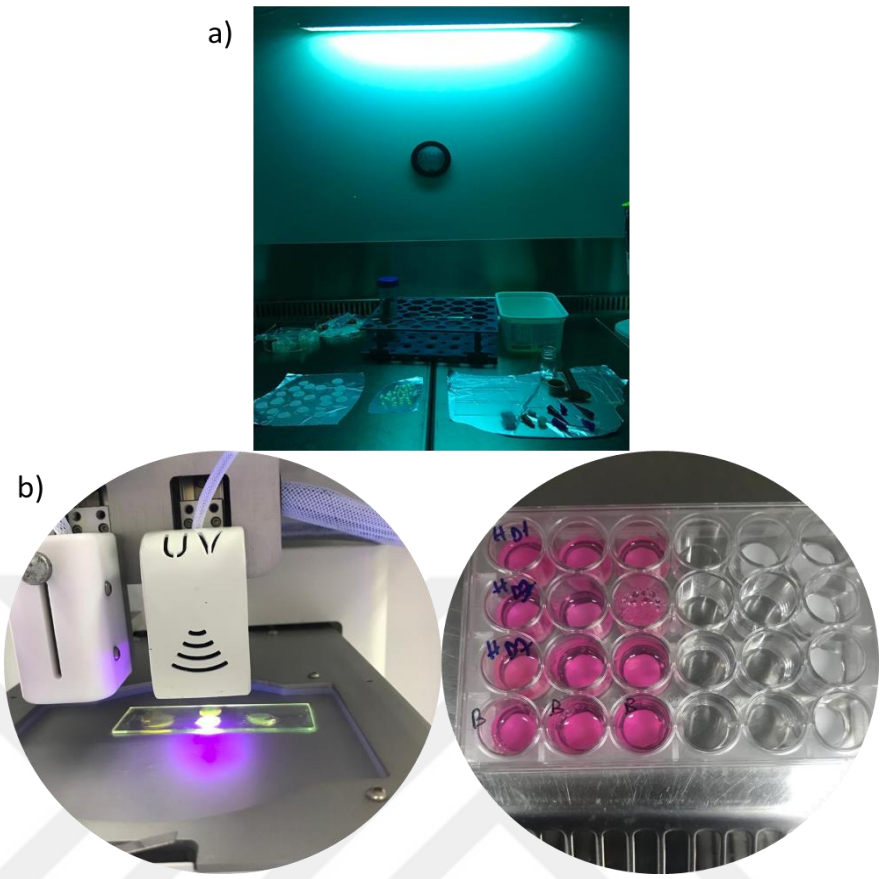

Figure 3.4 Preparation of scaffolds by 3D bioprinting method with cell-laden bioink using PUMA-6 a) Sterilization step b) The prepared samples were transferred to cell culture medium on Teflon holders after production and crosslinking

PUMA was also blended with GelMA and/or alginate to further improve cell attachment and viability within the bioink matrix. For this, PUMA-6 (within DMEM, Eosin Y, TEA and VP), was blended with GelMA. Alginate was used as a sacrificial material which was then removed from the structure (by enzymatic treatment with alginate lyase) to obtain a porous network. C2C12 cells were added into the polymers at a concentration of 2500 cells/µL. The bioink was then loaded into the print head of the 3D Bioplotter and the print parameters were adjusted using the Envisiontec 3D-Bioplotter software (**Figure 3.5**). Accordingly, while the pressure used for 3D printing is 2.5 bar, the print speed is 8.5 mm/s. The 3D printed samples were then kept under UV light for 3 minutes and then soaked in in 0.5 M $CaCl_2$ for 2 minutes to obtain the crosslinked hydrogel.

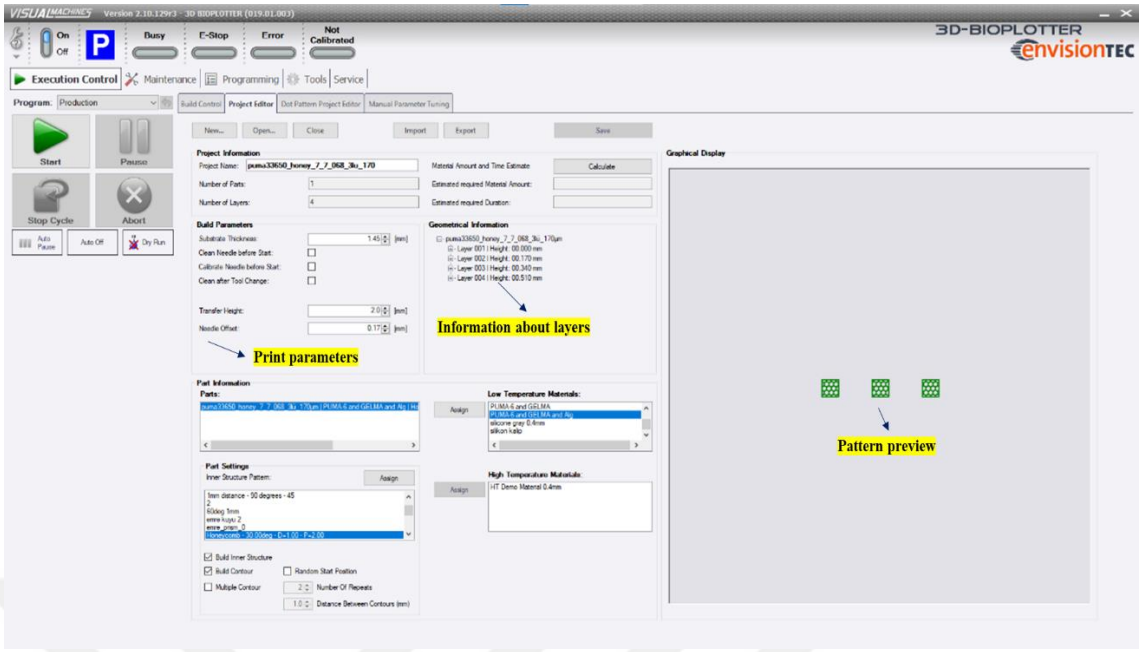

Figure 3.5 Design tab of Envisiontec Visual Machines software

3.2.4.5 Quantification of cell viability with Alamar Blue assay

Cell viability within the bioink matrix was assessed by the Alamar Blue cell proliferation assay. For this, cell-laden samples were rinsed with PBS at certain days of the culture. Alamar Blue solution prepared at 5% (v/v) in colorless low glucose DMEM was added to the wells containing the samples. They were then incubated for 1 hour in a dark environment in an incubator (37ºC and 5% CO_2). At the end of the period, 200 µL of test sample was taken from each well and transferred to 96-well microplates. The 96-well microplate was placed in the microplate reader and absorbance reading was performed at wavelengths of 570 nm-595 nm. The Alamar Blue solution in the wells containing the samples was removed and rinsed with PBS. Afterwards, fresh medium was added to the wells and culture was continued with the same samples. Absorbance values were converted to approximate cell number by means of a calibration curve determined for the used cells.

3.2.4.6 Phalloidin/DAPI staining

Phalloidin/DAPI staining was performed to examine the spread and morphology of cells within the scaffolds. On the 1st, 3rd and 7th days of culture, scaffolds were fixed at +4 ^{o}C for 4 hours using 3.7% (w/v) PFA solution. Afterwards, the fixed samples were rinsed twice with PBS solution, they were kept in Triton X for 5 minutes at room temperature. Scaffolds were treated with Triton X to prevent non-specific binding during staining via incubation in 1% BSA for 30 minutes at 37 ^{o}C and 5% CO_2 conditions in an incubator. Actin filaments were labeled with Phalloidin-FITC by incubation for 1 h at 37°C in a light-protected environment. After then, PBS was used for washing. Then, DAPI dye, which is used to mark the cell nuclei, was added to the tissue scaffolds that were washed with PBS twice and left at room temperature for 10 minutes. The samples were then rinsed with PBS and observed with a fluorescent microscope (Zeiss) and with a confocal laser scanning microscope (Zeiss). The wavelengths excitation/emission for DAPI was 340/488 nm, and for Phalloidin 495/518 nm.

4. RESULTS AND DISCUSSION

4.1 Optimization of PU-Based Photocrosslinkable Hydrogel Formation and 3D Printability

PU-methacrylic anhydride (MAA) and PU-maleic anhydride (MA) were synthesized and studied as photocurable hydrogel formulations.

PUMAA was prepared as described in Section 3.2.2. Then, TEA, VP and EY were added as photoinitiators to crosslink the polymer structure with visible (blue) light. An aqueous solution was prepared at concentrations of 6% w/v PUMAA, 1.88% v/v TEA, 1.25% v/v VP, 0.50 mM EY. The prepared solution was exposed to blue light at different time intervals. It was observed that crosslinking for 1 and 2 minutes was not enough to obtain a stable crosslinked network. When light illumination was extended for more than 3 min, it was observed that the samples started to dry out and efficient gelation could not be observed. **Figure 4.1** represents the crosslinking behavior of PUMAA with visible light.

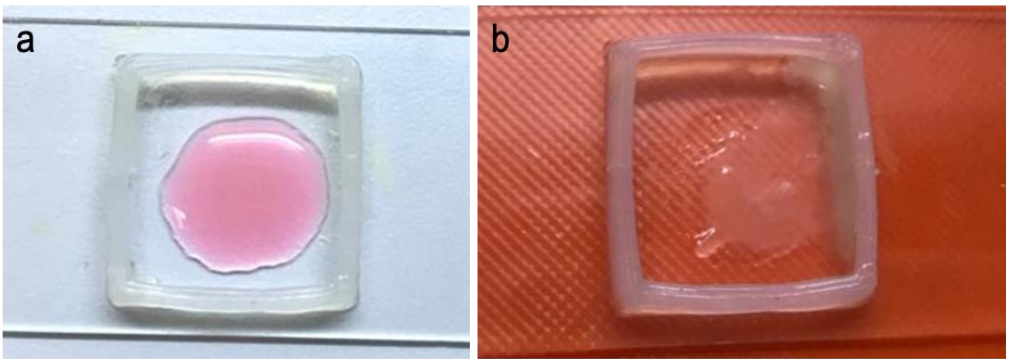

Figure 4.1 Structure of PUMAA hydrogel a) before, b) after exposure to blue light (470 nm) for 3 min

Similarly, PUMA photocrosslinking was studied and **Figure 4.2** represents the proper photo-crosslinking of the hydrogel matrix with visible light in 3 minutes, under similar experimental conditions.

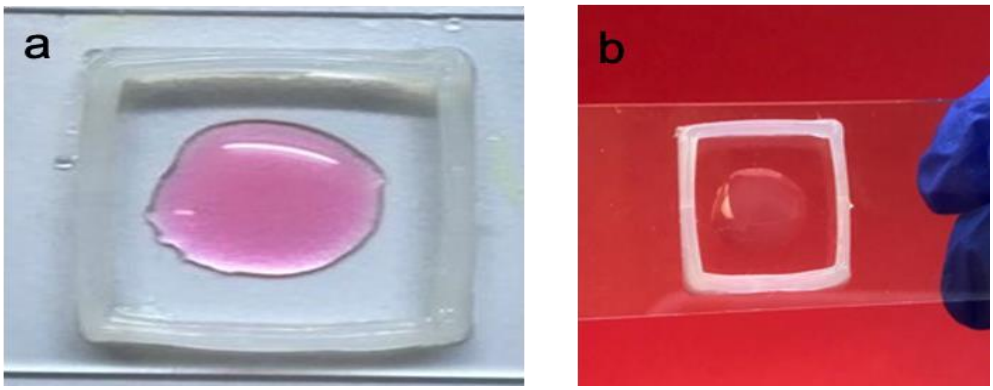

Figure 4.2 Structure of PUMA hydrogel a) before, b) after exposure to blue light (470 nm) for 3 min

Since PUMA showed superior potential of photo-crosslinking in these preliminary experiments, PUMAA was not used in the rest of the studies and photocrosslinkable PUMA hydrogel formation was further optimized with the parameters presented in **Table 3.5** (Polymer Type, Polymer Concentration, Photoinitiator Concentration, Light Source, Crosslinking time). Optimization was based on development of a hydrogel structure that has proper rheological properties for 3D printability, as well as proper structural stability upon crosslinking. The printability and crosslinking outcomes based on the hydrogel components are presented in **Table 4.1**.

Table 4.1 The printability and crosslinking outcomes based on the PUMA hydrogel components

Exp#	Material	Polymer Amount (g)	Water (g)	DM EM (µL)	Eosin Y (µL)	VP (µL)	TEA (µL)	Curing Conditions				Remarks	
								Vis. light (nm)	UV light (nm)	T (ºC)	Time (min)	Crosslinking (√ / X)	Stability (√ / X)
1	PUMA-2	0.43	1.50	-	250	43.75	65.62	470	-	24	5	X	X
2	PUMA-2	0.87	1.50	-	250	87.50	131.25	470	-	24	5	X	X
3	PUMA-2	1.31	1.50	-	250	131.25	196.87	470	-	24	5	X	X
4	PUMA-6	0.43	1.50	-	250	43.75	65.62	470	-	24	5	X	X
5	PUMA-6	0.87	1.50	-	250	87.50	131.25	470	-	24	5	X	X
6	PUMA-6	1.31	1.50	-	250	131.25	196.87	470	-	24	5	X	X
7	PUMA-33	0.43	1.50	-	250	43.75	65.62	470	-	24	5	X	X
8	PUMA-33	0.87	1.50	-	250	87.50	131.25	470	-	24	5	X	X
9	PUMA-33	1.31	1.50	-	250	131.25	196.87	470	-	24	5	X	X
10	PUMA-2	0.17	0.25	-	250	50	50	-	395	24	10	X	X
11	PUMA-6	0.20	0.30	-	250	50	50	-	395	24	10	√	X
12	PUMA-6	0.69	0.30	-	250	50	50	-	395	24	10	X	X
13	PUMA-6	0.69	0.30	-	500	100	100	-	395	24	15	√	X
14	PUMA-6	0.69	-	-	500	100	100	-	395	24	20	√	√
15	PUMA-6	0.69	-	-	566	100	100	-	395	24	10	√	√
16	PUMA-33-2 10%	0.07 PUMA-2 0.62 PUMA-33	-	-	566	100	100	-	395	24	10	X	√
17	PUMA-33-2 40%	0.27 PUMA-2 0.41 PUMA-33	-	-	566	100	100	-	395	24	10	X	√

Table 4.1 The printability and crosslinking outcomes based on the PUMA hydrogel components (continued)

18	PUMA-33-2 45%	0.31 PUMA-2 0.38 PUMA-33	-	-	566	100	100	-	395	24	10	X	√
19	PUMA-33-2 50%	0.34 PUMA-2 0.35 PUMA-33	-	-	566	100	100	-	395	24	10	medium	√
20	PUMA-33-6 40%	0.27 PUMA-6 0.41 PUMA-33	-	-	566	100	100	-	395	24	10	medium	√
21	PUMA-33-6 50%	0.34 PUMA-6 0.35 PUMA-33	-	-	566	100	100	-	395	24	10	√	√
22	PUMA-33-6 50%	0.34 PUMA-6 0.35 PUMA-33	-	250	250	70	105	-	395	24	20	√	√
23	PUMA-33-6 75%	0.52 PUMA-6 0.17 PUMA-33	-	250	250	70	105	-	395	24	20	√	√
24	PUMA-33-6 50%	0.25 PUMA-6 0.25 PUMA-33	-	250	250	70	105	-	395	24	20	√	√
25	PUMA-6	0.70 PUMA-6	-	250	250	70	105	-	395	24	20	√	√
26	PUMA-6	0.50 PUMA-6	-	250	250	70	105	-	395	24	20	√	√

Figure 4.3 depicts the steps followed for 3D printing and photo-crosslinking of PUMA-2, PUMA-6 and PUMA-33 polymers. In order to improve the cross-linking and printability properties, the polymer and photoinitiator concentrations were optimized. However, since the viscosities of the samples are low, even if the pattern is formed after 3D printing, deterioration of the pattern was observed within a few minutes after the print. In other words, printability was not proper since the viscosity was lower than needed. In addition, although the hydrogel structure started to form, the gelation of the material could not be achieved due to insufficient crosslinking.

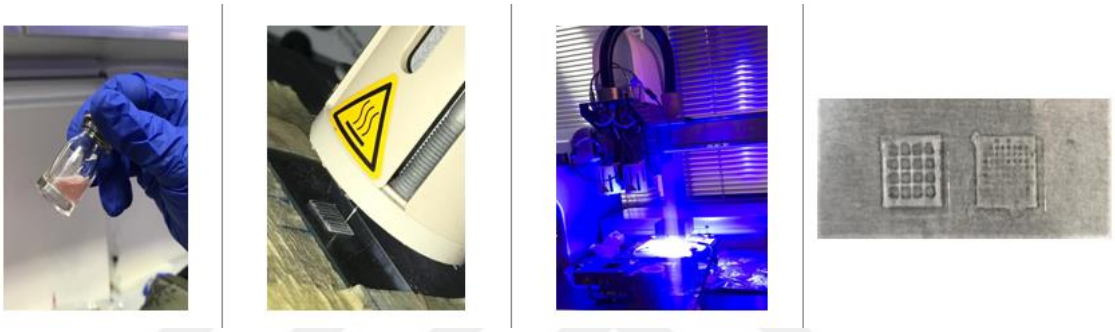

Figure 4.3 Studies to obtain bioinks with Eosin Y, VP and TEA in the presence of visible light

The optimization of polymer/photoinitiator concentration used to ensure photo-crosslinking with visible light did not reveal successful results, and proper gelling behavior could not be obtained. Therefore, UV light which has a higher energy compared to the blue light was used instead for the rest of the studies. Blue light has an average wavelength of 400 nm and above, while UV light generally has a wavelength between 365-395 nm (Noshadi et al., 2017; Zheng et al., 2021).

Representative images of hydrogel formation in the presence of EY, TEA and VP cured with UV light are shown in **Figure 4.4**. PUMA-6 was used instead of PUMA-2 to increase the viscosity of the polymer solution to enhance the gelation and crosslink behavior.

Parameters optimized included PUMA-6 concentration to increase the viscosity of the polymer solution as well as an increase in exposure time to UV light for 15 and 20 min.

It was observed that this enhanced light exposure duration is beneficial for efficient crosslinking. Further increase in the polymer concentration together with the use of increased UV-exposure time revealed better printability and gelation, as can be seen in **Table 4.1**, **Figure 4.4** and **Figure 4.5**.

Although a stable gel formation was obtained, cellular viability within this bioink matrix (results presented later) could not be achieved, probably due to very high stiffness of the matrix. Accordingly, printability/stability optimization studies were repeated by using PUMA-33, PUMA-2 and PUMA-6 blends at different ratios, which have higher viscosity (better printability) or better cross-linking (higher stability) properties in aqueous solution in accordance with their molecular weight/double bond characteristics.

Similarly, it was observed that the concentration of the photo-initators within the bioink matrix was affecting cellular viability; since the cytotoxicity analysis of the polymers vs. the bioink (polymer+photoinitiators) revealed contradictory results (data presented later) presented. Accordingly, it has been observed that the amount of photoinitiator or the amount of UV light may affect the toxicity (Qin et al., 2014). In this direction, photo-initiator amount was reduced.

3D printability and gelation properties as well as the matrix cytotoxicity were optimized with the parameters presented in **Table 4.1**. Afterwards, it was observed that the PUMA-33-6 bioink material optimized was not stable in the long-term within the cell culture media. Gelling property of the matrix was enhanced by increasing the amount of PUMA-6 or reducing the amount of total polymer. Since PUMA-6 was found to be stable in the cell culture medium for 4 days, with proper 3D printability, gelling and cytotoxicity properties; this material was used in further cell culture studies with the bioink formulation: 0.50 g PUMA-6, 250 μL DMEM, 250 μL EY, 105 μL TEA and 70 μL VP formulation as given in **Table 4.1.**

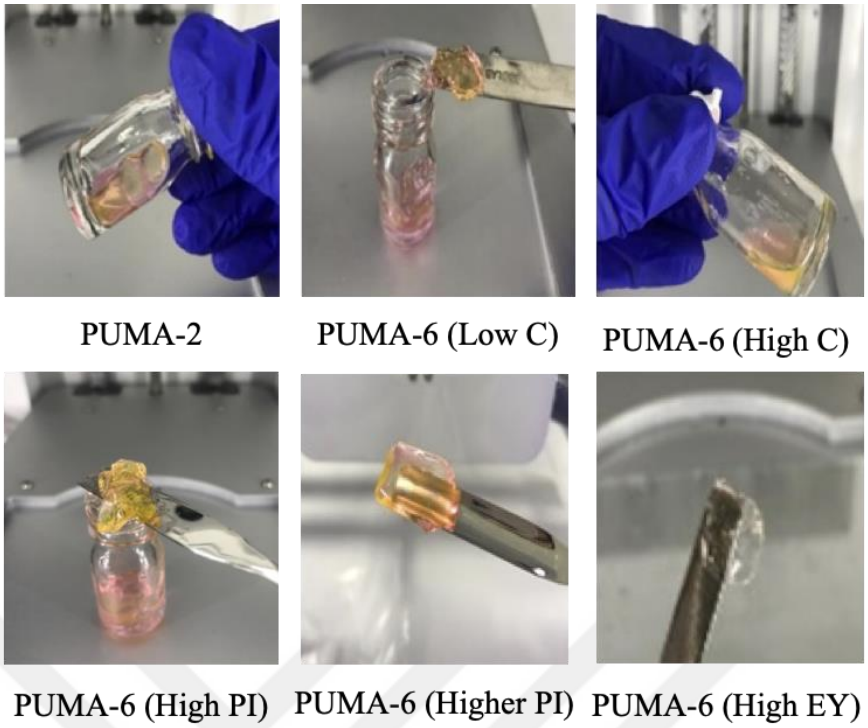

Figure 4.4 Optimization of PUMA hydrogel formation in the presence of EY, TEA and VP using UV light. C: Concentration, PI: Photoinitiator, EY: Eosin Y

Figure 4.5 Optimization of PUMA blend hydrogel formation in the presence of EY, TEA and VP using UV light. PI: Photoinitiator

In the 3D printing studies carried out with PUMA-33-6 (high PI), cross-linking was achieved with 10 minutes of UV light exposure. The samples obtained and the 3D printing procedure applied is shown in **Figure 4.6**.

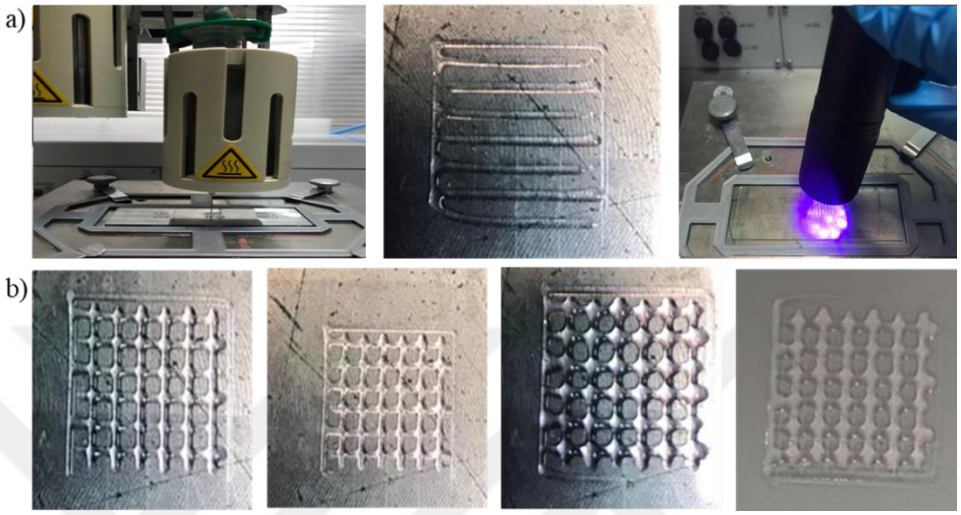

Figure 4.6 3D printing with PUMA-33-6 (high PI) a) 2 minutes curing with UV light after single layer printing b) Samples produced in two layers showing moderate print fidelity

3D printing with PUMA-33-6 (low PI) revealed similar print fidelity as compared to the high PI use, as shown in **Figure 4.7**.

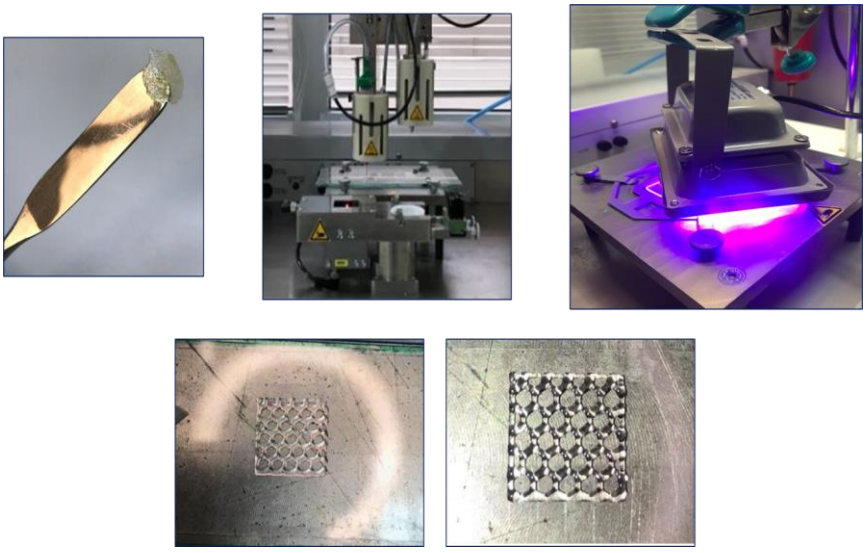

Figure 4.7 3D bioprinting process with PUMA-33-6 (low PI)

4.2 Material Characterization

4.2.1 FTIR spectra of PUMAA and PUMA

FTIR analysis for PUMAA and PUMA showed a strong hydrogen bonded urea C=O band at 1620 cm^{-1}, as expected, in all polymers. While the amide C=O band with hydrogen bonding at 1633 cm^{-1} gave a significant peak in PUMA and reference PUMA, a weak peak was observed in PUMAA. In addition, -COOH band was observed at 1718 cm^{-1} in PUMA and reference PUMA. The FTIR spectra given in **Figure 4.8** show that PUMA synthesis is more successful as a result of the reaction performed with MA, while the reaction with MAA also occurs, but it is also shown with FTIR that it is less successful compared to MA.

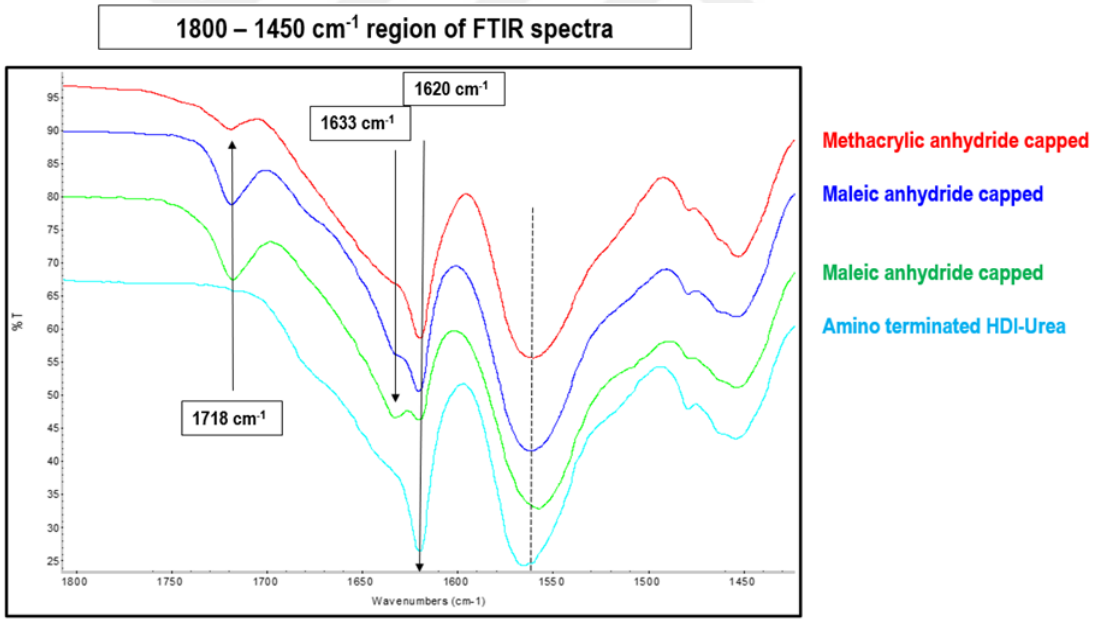

Figure 4.8 FTIR spectra of PU (blue spectrum), PUMAA (red spectrum), PUMA (green spectrum), and reference PUMA (dark blue spectrum) polymers

4.2.2 FTIR spectra of photo-crosslinked hydrogels

The FTIR analysis results of the hydrogels show that the ether peak from PUMA-6 emerges at 1100 cm^{-1} on all samples except GelMA. All samples show amide I (strongly hydrogen bound carbonyl) at 1633 cm^{-1} and amide II (N-H bending) at 1539 cm^{-1}. Amide III peaks can be found between 1200 and 1400 cm^{-1}. According to these data (**Figure 4.9**), the ether peak was observed in other groups except the GelMA group, indicating that the reactions with PUMA-6 were successful. The fact that the values seen in GelMA are also included in other groups containing GelMA proves that the reactions with GelMA are also successful.

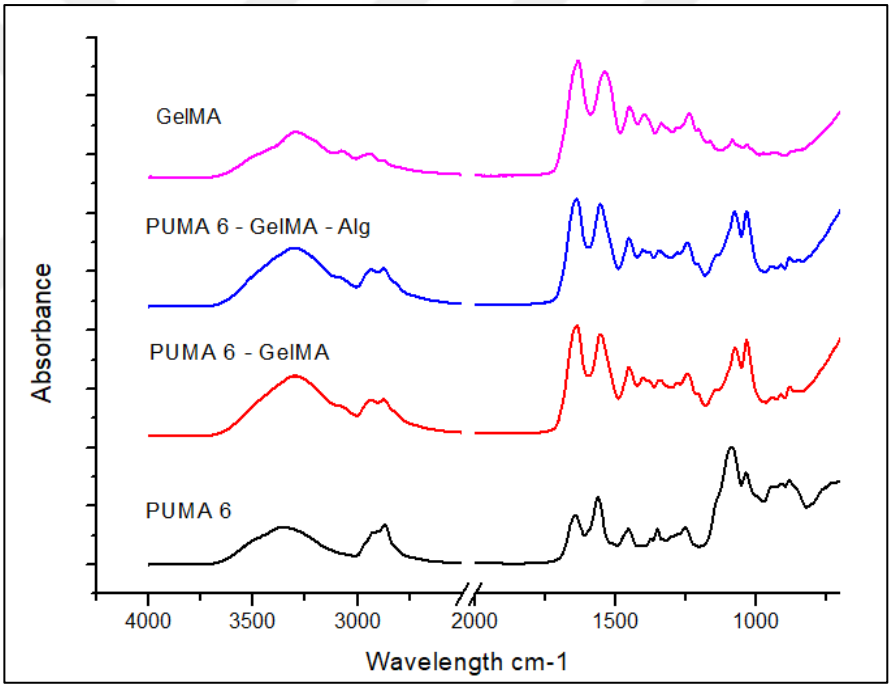

Figure 4.9 FTIR spectra of Photo-Crosslinked Hydrogels

4.2.3 Viscosity of the bioinks

PUMA-6 was blended with GelMA and/or alginate to increase cellular viability as well as the matrix stiffness and porosity (alginate as the sacrificial bioink) in the bioink

optimization studies. Therefore, rheological characterization of these samples were performed.

Figure 4.10 shows the viscosity of the samples of PUMA-6, PUMA-6/GelMA blend and PUMA-6/GelMA/Alg blend samples with the photoinitiators used to prepare the bioinks. It was observed that a decrease in dynamic viscosity was observed as shear rate increased. It is thought that the instant viscosity increase in the PUMA-6/GelMA blend sample is due to the inhomogeneity at the time of measurement. The viscosity profile that decreases as the shear rate increases in PUMA-6/GelMA blend and PUMA-6/GelMA/Alg blend samples coincides with the rheological behavior of bioink properties in the literature (Hölzl et al., 2016). Viscosity values are also within the printability limits accepted in the literature (Hölzl et al., 2016). The viscosity of the PUMA-6 sample alone was below the printability limit when compared to the other samples.

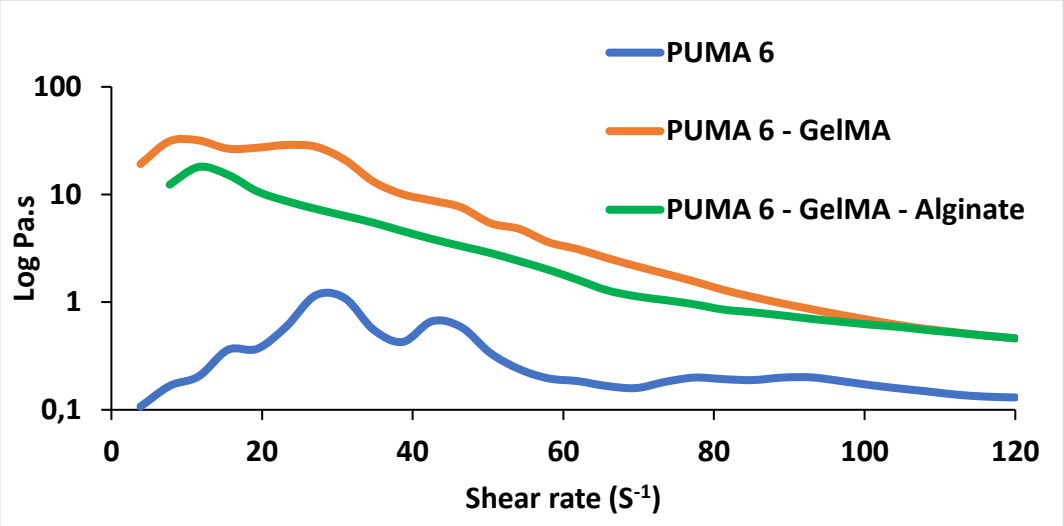

Figure 4.10 Viscosity of PUMA-6, PUMA-6/GelMA and PUMA-6/GelMA/Alg bioinks

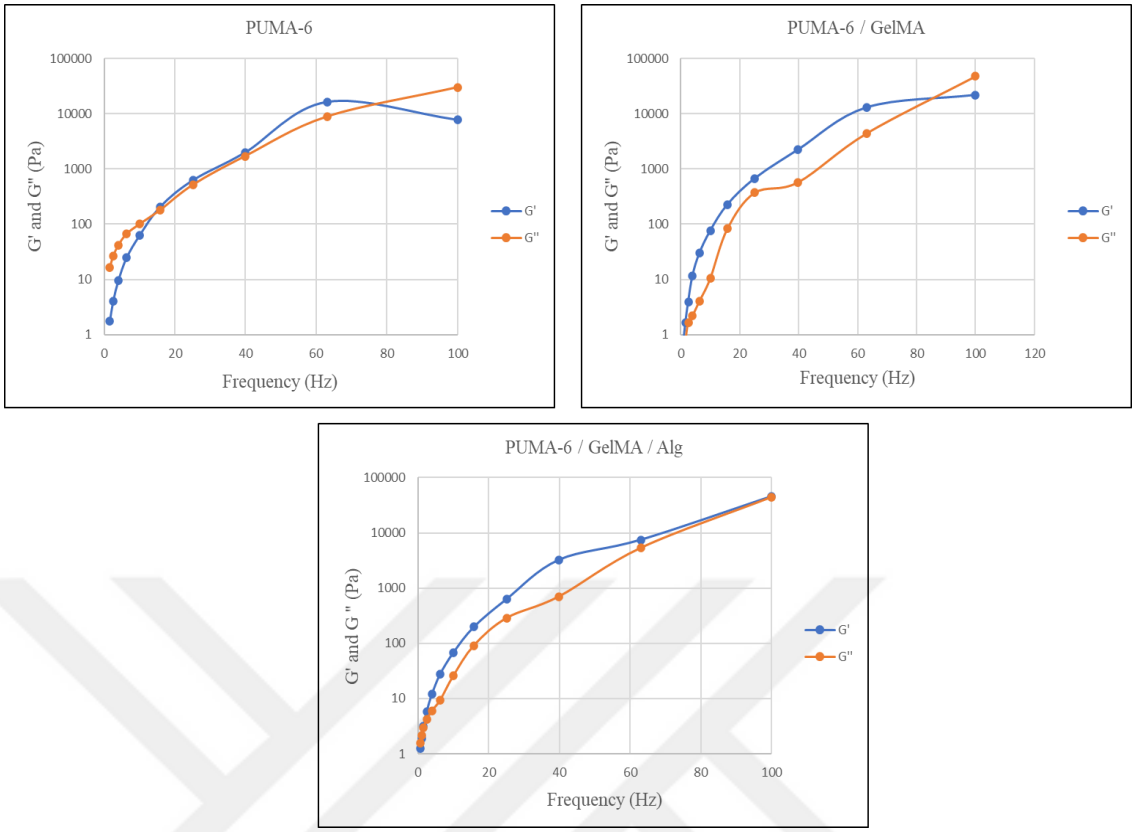

Figure 4.11 The storage (G') and loss modulus (G") profiles of PUMA-6, PUMA-6/GelMA and PUMA-6/GelMA/Alg bioinks

Figure 4.11 shows the storage (G') and loss modulus (G") profiles of developed polymers. In low frequency ranges, the storage modulus of PUMA-6 is lower than the loss modulus. As the frequency increases, the storage modulus has a higher value than the loss modulus and there is an increase in the loss modulus towards 100 Hz. Looking at the PUMA-6/GelMA modulus profiles, the storage modulus is higher than the loss modulus in low frequency ranges. As the frequency increases, the storage modulus continues at higher values than the loss modulus, and the loss modulus increases towards 100 Hz. In the low frequency ranges, PUMA-6/GelMA/Alg exhibits a similar profile to PUMA-6/GelMA. As the frequency increases, as in PUMA-6/GelMA, the storage modulus continues at higher values than the loss modulus and it is seen that the storage modulus and loss modulus intersect towards 100 Hz.

The fact that the storage modulus is higher than the loss modulus indicates the susceptibility to elastic behaviour, and the lowness indicates the susceptibility to viscous

behaviour. In the light of these data, the viscoelastic properties of the developed polymers were investigated.

4.2.4 Mechanical properties of the bioinks

Table 4.2 presents the Young's Modulus values of the films obtained from the bioinks (PUMA-6, PUMA-6/GelMA and PUMA-6/GelMA/Alg). It was observed that the Young's modulus of the GelMA film was 5.02 MPa, while that of PUMA-6 film was 0.70 MPa, which is much better suited for soft tissues such as skeletal muscle. The Young's modulus of the film prepared with PUMA-6/GelMA was 3.14 MPa. Addition of Alg to this matrix reduced the Young's Modulus to 2.64 MPa.

Young's Modulus is defined as the ratio of stress to strain applied to a material. This also gives information about the elasticity of the material (Davis J. R., 2004). If a material has a high Young's modulus, it is interpreted that this material is stiffer and more resistant to stretching. In other words, materials with low Young's modulus can stretch more easily (Callister William D. & Rethwisch David G., 2018). Therefore, among these films, GelMA has the highest value, while PUMA-6 has the lowest value, indicating that PUMA-6 has a more elastic structure. The reduction of Young's modulus in the presence of Alg indicates better suitability with the intended application in skeletal muscle. In sum, among the bioink materials tested, PUMA-6 has the most suited mechanical properties.

According to the Ultimate Tensile Strength (UTS) data given in **Table 4.2**, it is seen that the lowest value is in the GelMA group. While the PUMA-6 group had higher values than GelMA, the blends had the highest values. It is seen in the **Table 4.2** that the elongation break percentages are proportional to the Young's Modulus values. Accordingly, PUMA-6 has the highest elongation at break and proves to be more elastic than other groups. While GelMA alone has the lowest elongation at break, it is seen that the elongation at break increases in groups where PUMA-6 is blended. As a result, the elasticity of PUMA-6 increased the elongation at break percentage of the blends.

Table 4.2 Tensile properties of the bioinks

	Young's Modulus (MPa)	Ultimate Tensile Strength (MPa)	Elongation at break (%)
GelMA	5.02 (± 0.17)	0.07 (± 0.005)	653
PUMA-6	0.70 (± 0.08)	0.10 (± 0.04)	913
PUMA-6/GelMA	3.14 (± 0.24)	0.29 (± 0.04)	800
PUMA-6/GelMA/Alg	2.64 (± 0.29)	0.23 (± 0.03)	865

4.2.5 SEM analysis

The morphology of the hydrogels were examined by SEM imaging. When the 3 groups are compared, it is seen that PUMA-6/GelMA/Alg blend and PUMA-6/GelMA blend have comparable porous architecture compared to PUMA-6 (**Figure 4.12**). The porosity in the matrix is expected to increase when the Alg component within the matrix is removed following treatment with alginate lyase.

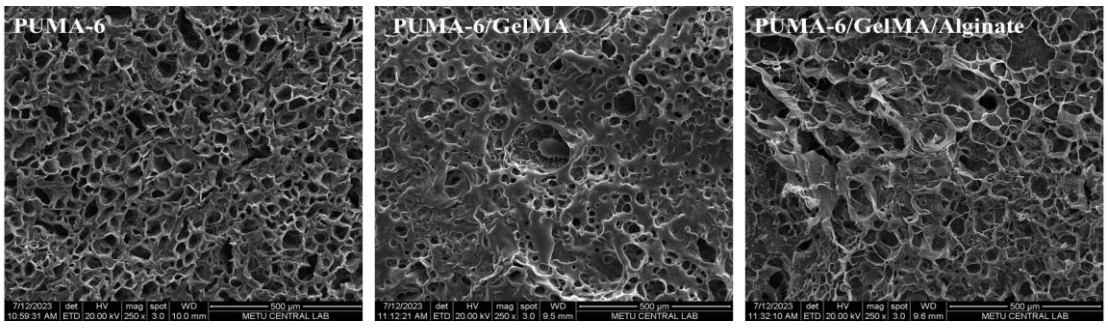

Figure 4.12 SEM images of the PU-based hydrogels and blends (Scale bar: 500μm)

4.3 *in vitro* Studies

4.3.1 Cytotoxicity assessment of PUMA polymers

Cell layer spread and the amount of dead cells were examined at 10x magnification with phase contrast microscope at 24 and 48 hours after the addition of the extraction liquid, according to the experimental groups. The cell layer spread observed at 24 and 48 hours is given in **Figure 4.13**. Changes in cell morphology observed throughout the culture were examined at 40x magnification and the results are presented in **Figure 4.13**. The amount of cells and cell inhibition in the samples by Alamar Blue Test performed as a result of the experiment are shown in **Figure 4.14** and **Figure 4.15**, respectively.

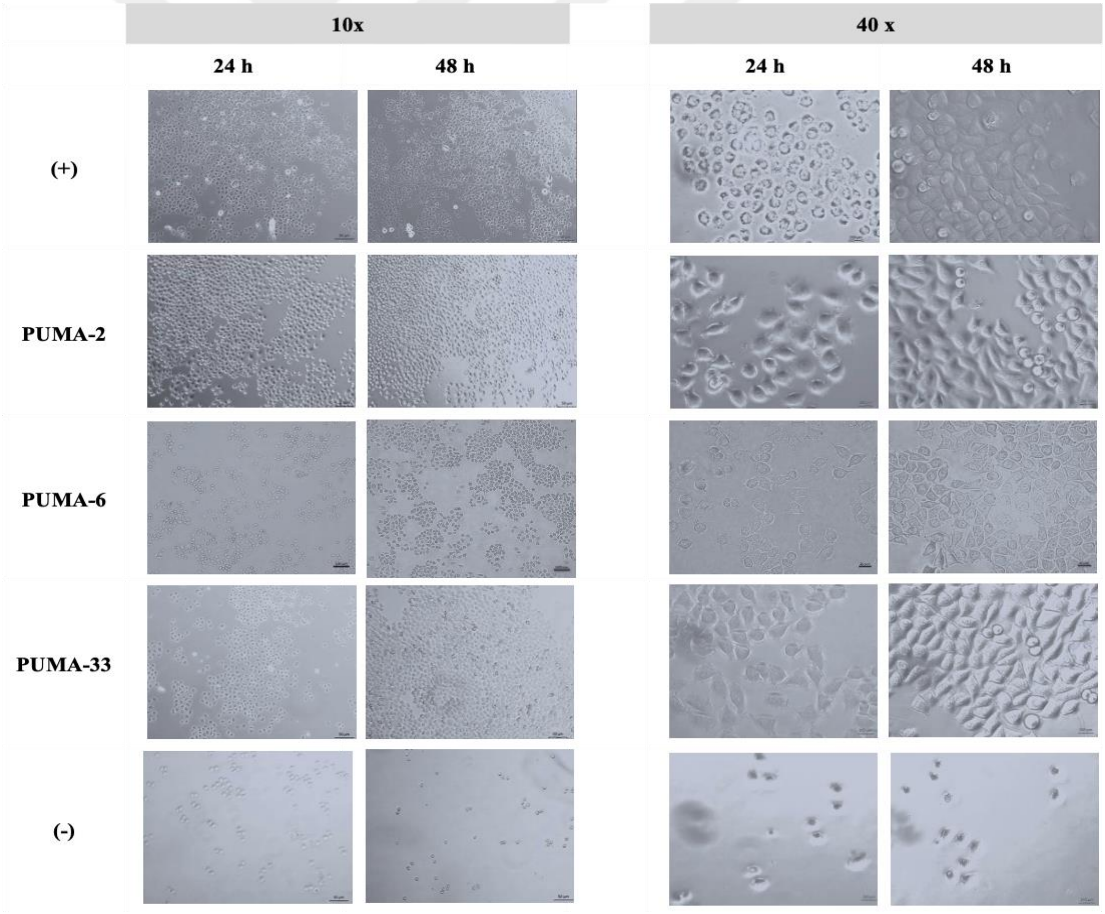

Figure 4.13 Change of cell layer spread (10x) and cell morphology (40x) at 24 and 48 hours after addition of extraction liquid in the cytotoxicity test of PUMA polymers

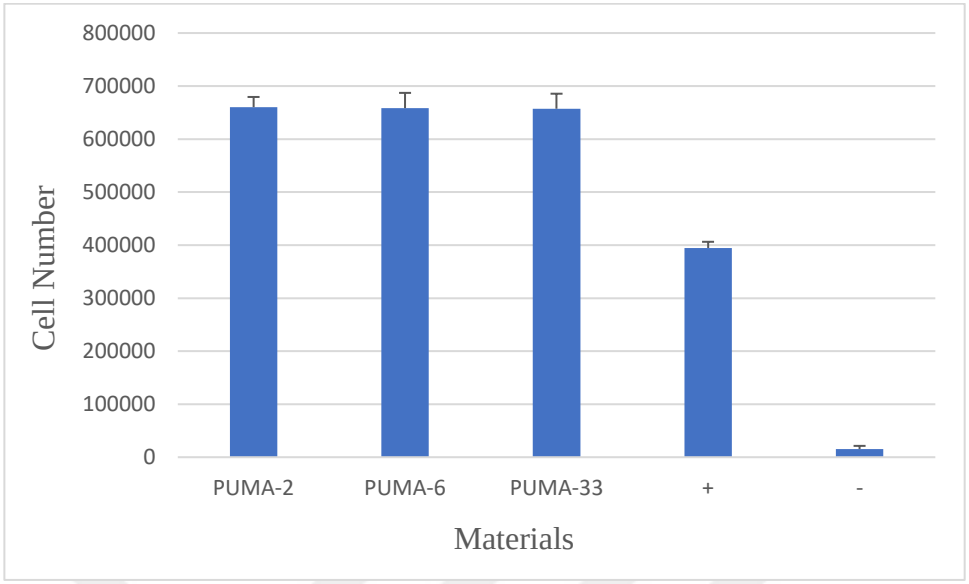

Figure 4.14 Viable cell number in the cytotoxicity test of PUMA polymers determined by Alamar Blue assay

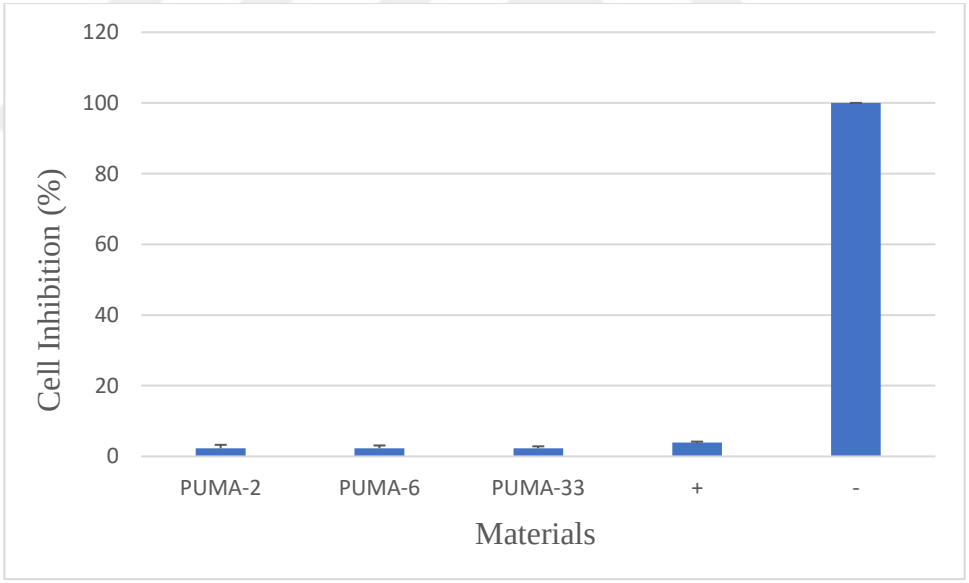

Figure 4.15 Inhibition of cell growth in the cytotoxicity test of PUMA polymers

According to the microscopic examination, the results of the experimental groups according to the "cytotoxicity test evaluation criteria" scoring scale given in section 3.2.4.1 are presented in **Table 4.3**. According to these results, the cytotoxic response

index and cytotoxicity evaluation results for materials are presented in **Table 4.4**. These results show that the PUMA polymers do not contain cytotoxic leachables.

Table 4.3 Cytotoxicity test evaluation criteria results for PUMA polymers

	Sample	Grade		Sample	Grade
Cell layer spread (Confluency)	PUMA-2	1	**Change in cell morphology**	PUMA-2	1
	PUMA-6	1		PUMA-6	1
	PUMA-33	1		PUMA-33	1
Amount of dead cells (Floating cells)	PUMA-2	1	**Cell growth inhibition**	PUMA-2	0
	PUMA-6	1		PUMA-6	0
	PUMA-33	1		PUMA-33	0

Table 4.4 Cytotoxicity assessment results for PUMA polymers

Sample	Cytotoxic Response Index	"Material is cytotoxic."
PUMA-2	1	No
PUMA-6	1	No
PUMA-33	1	No

4.3.2 Cytotoxicity assessment of the bioinks

Cell layer spread and the amount of dead cells were examined at 10x magnification with phase contrast microscope at 24 and 48 hours after the addition of the extraction liquid, according to the experimental groups. The cell layer spread observed at 24 and 48 hours is given in **Figure 4.16**. Changes in cell morphology observed throughout the culture were examined at 40x magnification and the results are presented in **Figure 4.16.** The amount of cells and cell inhibition in the samples by Alamar Blue Test performed as a result of the experiment are shown in **Figure 4.17** and **Figure 4.18**, respectively.

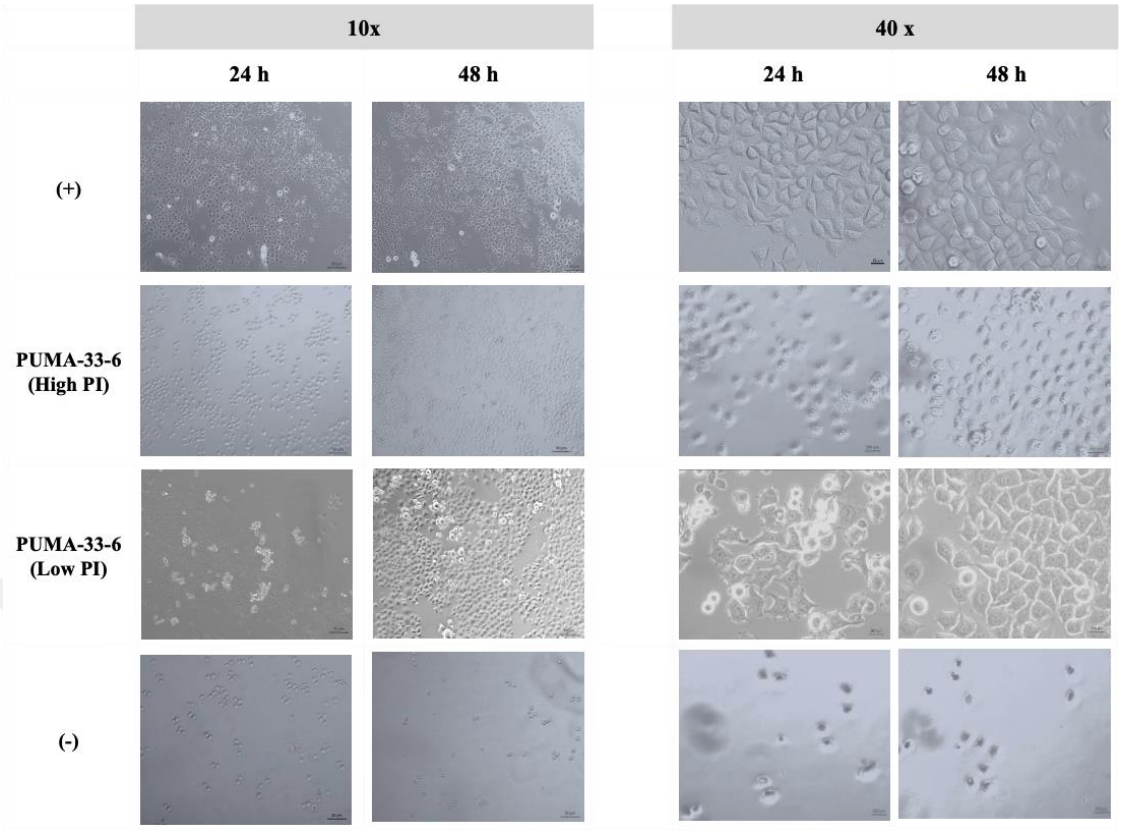

Figure 4.16 Change in cell layer spread (10x) and cell morphology (40x) at 24 and 48 hours after addition of extraction liquid in the cytotoxicity test of PUMA-33-6 bioink. PI: Photoinitiator

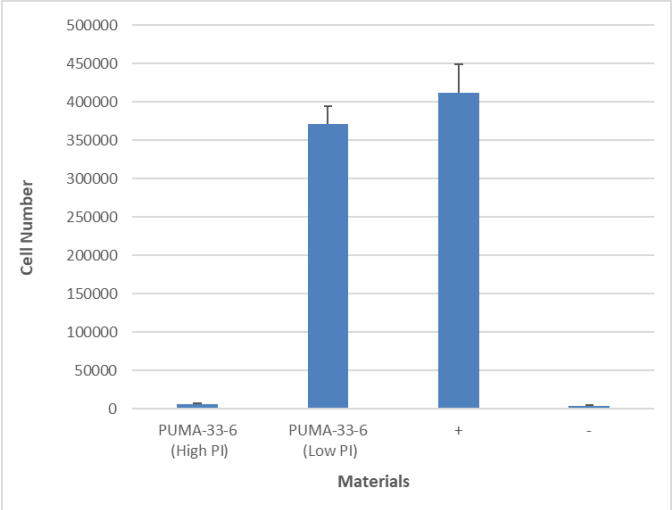

Figure 4.17 Viable cell number in the cytotoxicity test determined by Alamar Blue assay in the cytotoxicity test of PUMA-33-6 bioink. PI: Photoinitiator

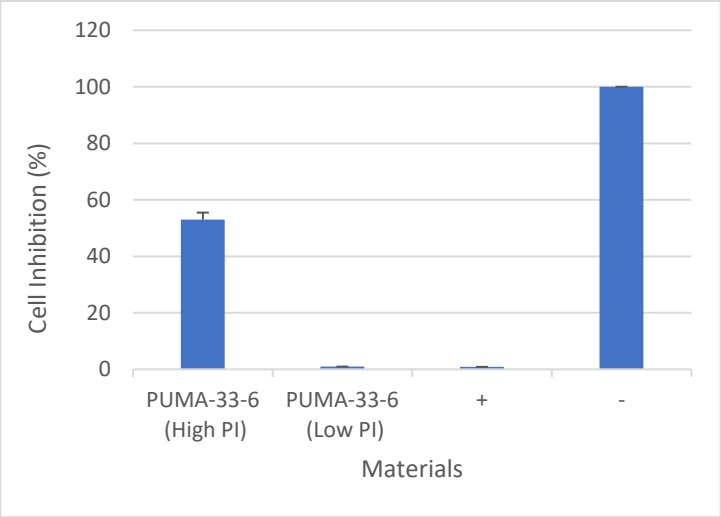

Figure 4.18 Inhibition of cell growth in the cytotoxicity test of PUMA-33-6 bioink. PI: Photoinitiator

According to the microscopic examination, the results of the experimental groups according to the "cytotoxicity test evaluation criteria" scoring scale given in section 3.2.4.1 are presented in **Table 4.5**. According to these results, the cytotoxic response index and cytotoxicity evaluation results for materials are presented in **Table 4.6**. These findings indicate that PUMA-33-6 (high PI) bioinks have a toxic effect, whereas PUMA-33-6 (low PI) bioinks do not.

Table 4.5 Cytotoxicity test evaluation criteria results for PUMA-33-6 bioink. PI: Photoinitiator

	Group	Grade		Group	Grade
Cell layer spread (Confluency)	PUMA-33-6 (High PI) bioink	3	**Change in cell morphology**	PUMA-33-6 (High PI) bioink	3
	PUMA-33-6 (Low PI) bioink	2		PUMA-33-6 (Low PI) bioink	2
Amount of dead cells (Floating cells)	PUMA-33-6 (High PI) bioink	4	**Cell growth inhibition**	PUMA-33-6 (High PI) bioink	4
	PUMA-33-6 (Low PI) bioink	2		PUMA-33-6 (Low PI) bioink	1

Table 4.6 Cytotoxicity assessment results for PUMA-33-6 bioink. PI: Photoinitiator

Group	Cytotoxic Response Index	"Material is cytotoxic."
PUMA-33-6 (High PI) bioink	7.3	Yes
PUMA-33-6 (Low PI) bioink	3	No

4.3.3 Cell viability within photocrosslinkable bioinks following bioprinting

Cell culture studies were performed with various PUMA-blends listed in **Table 4.7.** Parameters including the bioink viscosity, printability, gelation, durability, as well as cell adhesion and proliferation were considered to optimize the bioink composition.

Table 4.7 PUMA blends studied for the optimization of photo-crosslinkable bioink composition

#	Sample	Polymer (g)	Water (mL)	DMEM (µL)	Eosin Y (µL)	VP (µL)	TEA (µL)	P/S (µL)	Curing Conditions		
									UV light (nm)	T (ºC)	Time (min)
1	PUMA-6	0.69	-	-	566	100	100	-	395	24	10
2	PUMA-33-6	0.34 PUMA-6 0.35 PUMA-33	-	-	566	100	100	-	395	24	10
3	PUMA-33-6	0.34 PUMA-6 0.35 PUMA-33	-	250	250	70	105	-	395	24	20
4	PUMA-6	0.50	-	250	250	70	105	-	395	24	20
5	PUMA-6 GelMA	0.50 PUMA-6 0.50 GelMA	-	250	250	70	105	-	395	24	3
			2	-	500	25	37.50	20	395	24	
6	PUMA-6 GelMA Alg	0.50 PUMA-6 0.50 GelMA 0.02 Alg	-	250	250	70	105	-	395	24	5
			2	-	500	25	37.50	20	395	24	
			-	-	-	-	-	-	395	24	

PUMA-6 (high PI) bioink was used to bioprint cell-laden constructs and DAPI staining was performed at days 1, 3 and 7 of the culture to monitor cell proliferation within the matrix (**Figure 4.19)**. Results showed that the cell distribution in the bioink was not as uniformly distributed as expected. Therefore, it was decided that both the rheological properties of the bioink and the amount of cellular content should be optimized.

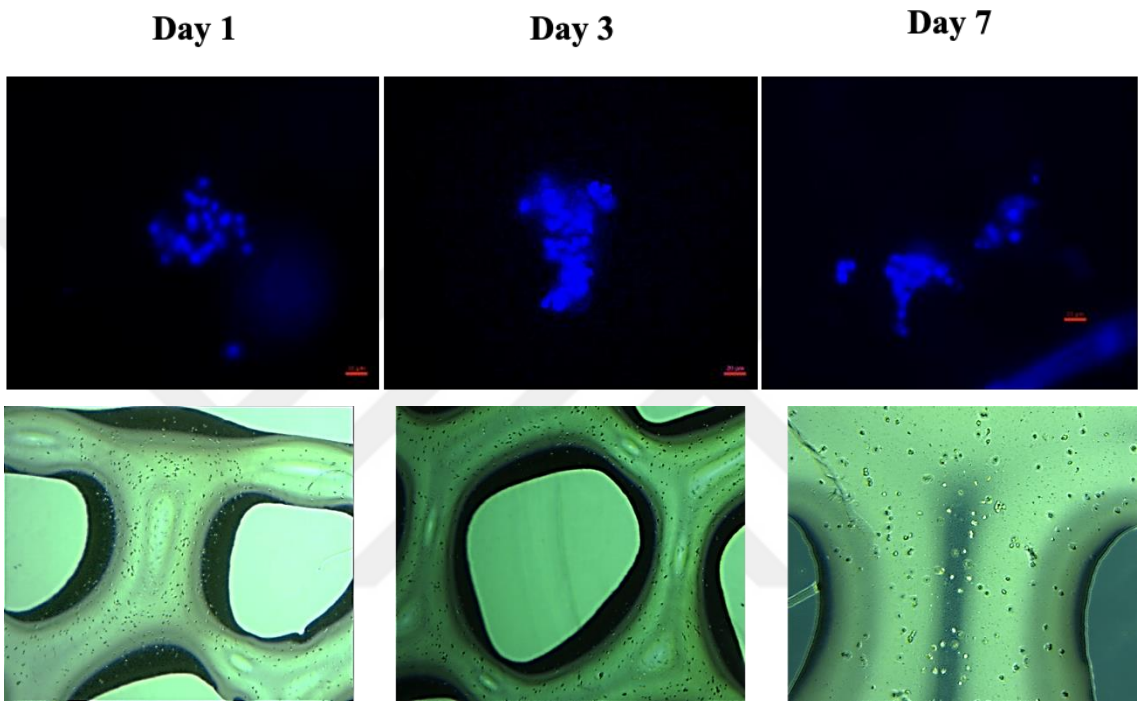

Figure 4.19 DAPI staining (upper row; 40x, Scale bar: 20 μm) and light microscopy images (lower row; 4x, 10x, 20x) to observe the presence of cells within PUMA-6-based bioink

PUMA-33-6 (high PI) blend was used with the C2C12 cells at various cell densities (1250, 2500 and 5000 cells/μL). Alamar Blue analysis was performed to quantify the number of viable cells within the bioink matrix (**Figure 4.20).** Although the results were not statistically significant, the highest cell proliferation rate was observed with the 2500 cells/μL samples on the 7th day. For this reason, the rest of the studies were conducted by using this cell concentration.

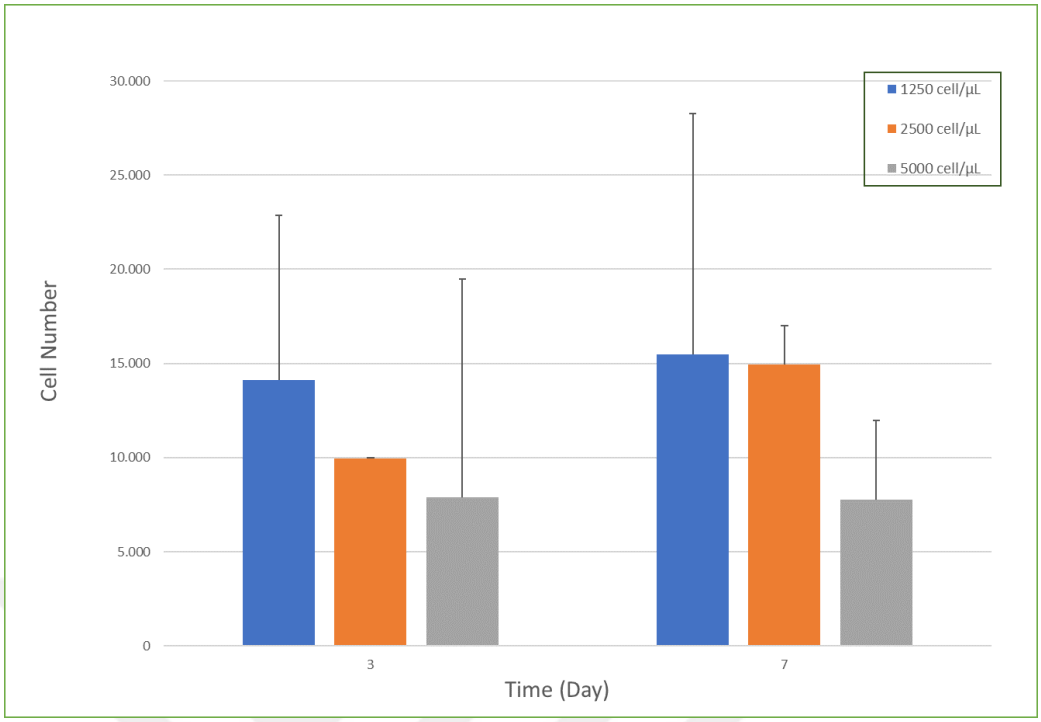

Figure 4.20 Cell viability analysis (Alamar Blue) results in the experiment performed to optimize the density of the cells to be used in the bioink

Light microscope images of cells within the PUMA-6 (low PI) bioink matrix in the culture following 3D bioprinting is shown in **Figure 4.21**. Phalloidin/DAPI staining evaluation done by fluorescence (**Figure 4.22**) and confocal laser scanning microscopy (**Figure 4.23**) were performed on day 7. Alamar Blue (**Figure 4.24**) analyzes were performed on days 1, 3 and 7.

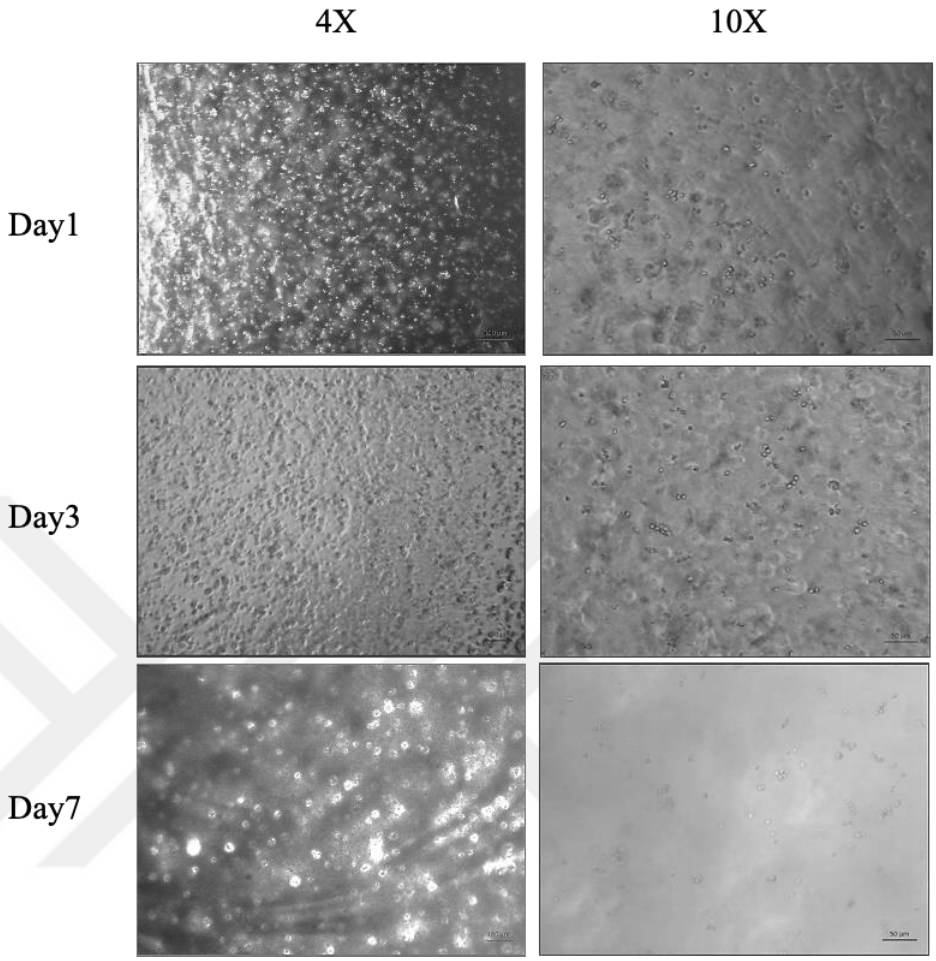

Figure 4.21 Light microscope images of cells within the PUMA-6 (low PI) bioink during the culture

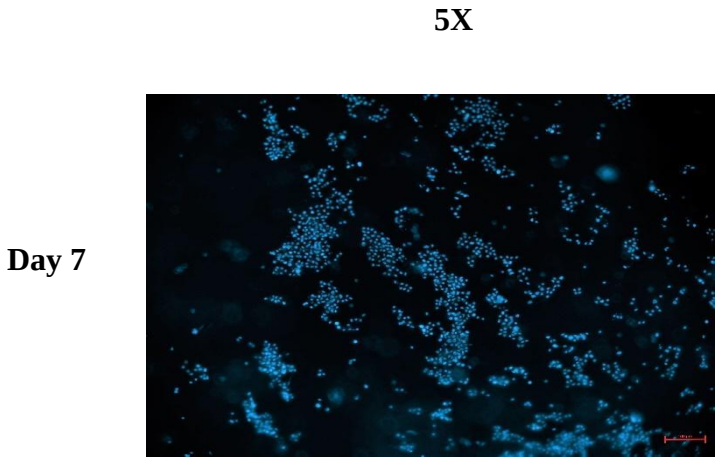

Figure 4.22 DAPI staining of C2C12 cells within PUMA-6 bioink (day 7)

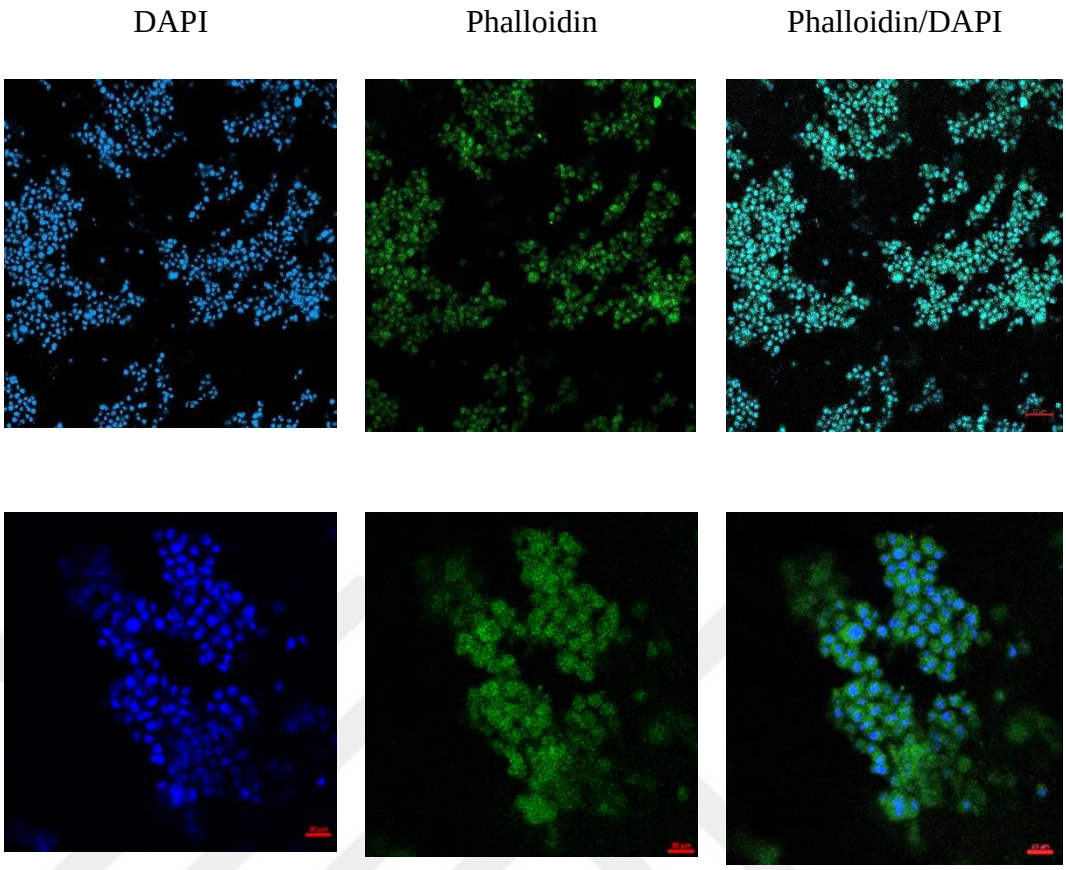

Figure 4.23 Confocal Laser Scanning Microscopy imaging of C2C12-laden PUMA-6 bioink on Day 7. 5x and 20x magnification. Scale bar = 50µm and 20µm. Channels: Phalloidin (green) and DAPI (blue)

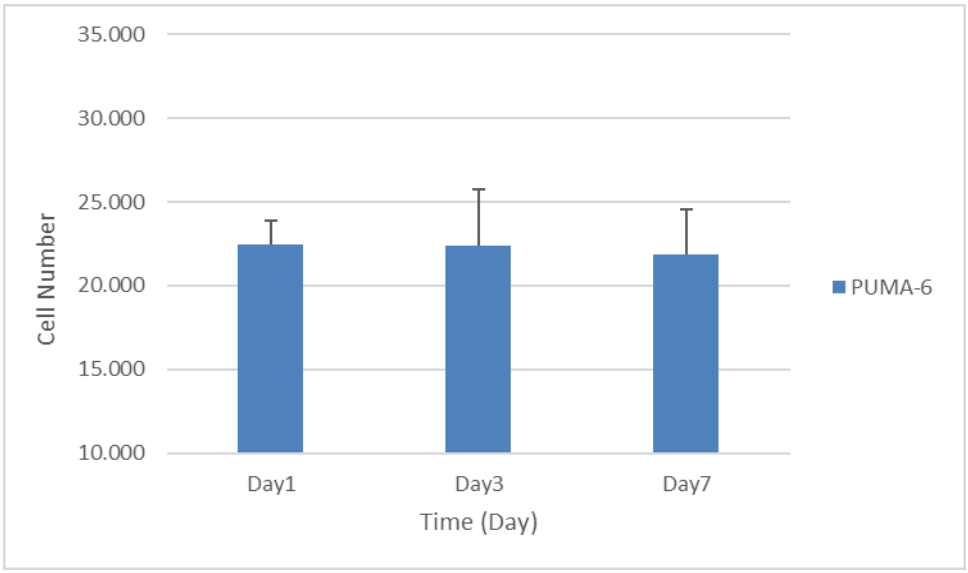

Figure 4.24 Assessment of cell viability with Alamar Blue assay within PUMA-6 bioink during culture

Light microscopy investigation presented in **Figure 4.21** did not provide proper observation of cellular presence and sprouting, probably due to the dense material matrix. In the immunofluorescence staining performed to label the actin filaments (counterstained with DAPI) (**Figures 4.22** and **4.23)** the presence of viable cells were clear, however the desired cell sprouting was not observed. Similarly, an increase in the cell proliferation rate was not observed in the quantification of cellular viability with Alamar Blue assay **(Figure 4.24)**. Therefore, it was hypothesized that the material chemistry (lack of cell binding domains) or physical properties (high stiffness and lack of proper porosity) could be the potential reasons for these results.

In order to overcome the above-mentioned problems, PUMA-6 was blended with GelMA and alginate (sacrificial). DAPI staining shown in **Figure 4.25**, and Phalloidin/DAPI staining data shown in **Figure 4.26** revealed the presence of viable cells. Quantification of viable cells with Alamar Blue analysis (**Figure 4.27**) showed an increase in the viable cell number within the PUMA/GelMA bioink matrix on day 7. Therefore, addition of biological components (gelatin) within the PUMA-6 matrix supported cellular viability. Moreover, since GelMA is also prone to photo-croslinking with the photoinitiators used under UV light, a stable gel matrix was obtained in much less UV exposure durations (3 min as compared to 20 min). This also was beneficial for the enhancement of cellular viability and proliferation since the potential DNA damage caused by UV light could be reduced, as well.

PUMA-6 / GelMA **5X**

Day 7

Figure 4.25 DAPI staining for PUMA-6/GelMA bioink including the C2C12 cells (day 7)

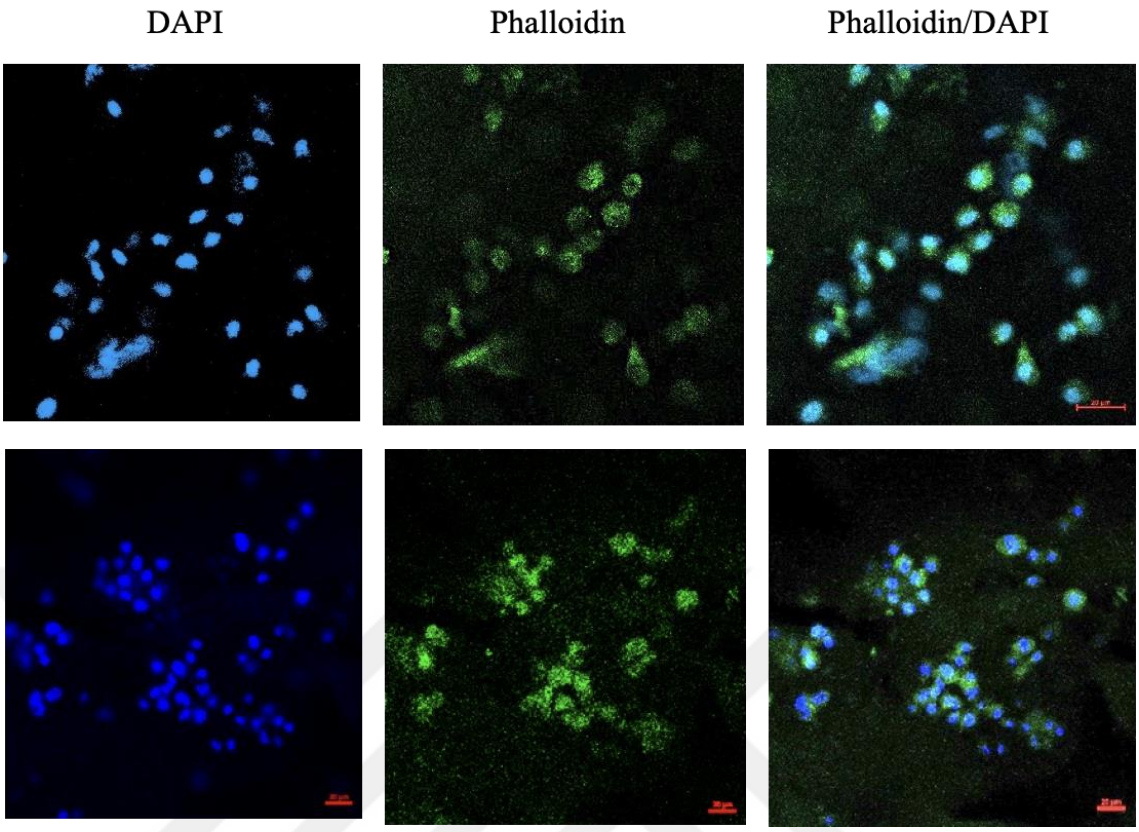

Figure 4.26 Confocal Laser Scanning Microscopy imaging of PUMA-6/GelMA bioink including C2C12 cells on Day 7. 20x magnification. Scale bar = 20µm. Phalloidin (green) and DAPI (blue)

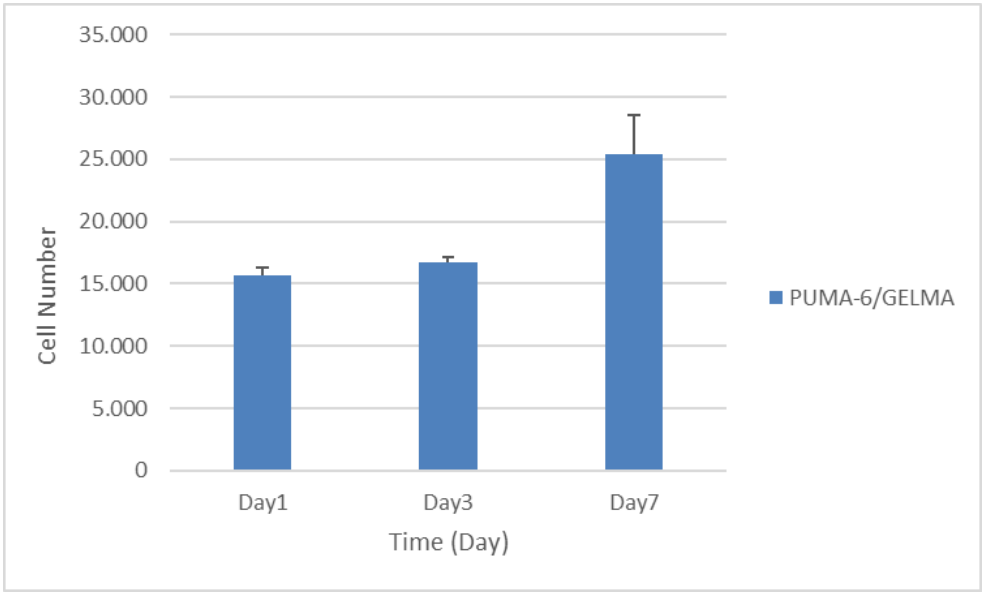

Figure 4.27 Assessment of cell viability with Alamar Blue assay within PUMA-6/GelMA bioink during culture

In order to further enhance the cellular viability, and especially sprouting, within the bioink matrix; PUMA-6/GelMA/Alg blends were prepared, in which alginate served as the sacrificial component. Results of cell culture study within this matrix are presented in **Figure 4.28** and **Figure 4.29** (Phalloidin/DAPI staining), during 7 day of culture.

In these studies, alginate was removed from the structure upon production by enzymatic treatment (alginate lyase). The enzyme concentration at two different concentrations; 0.05 U/mL and 1 U/mL. **Figure 4.30** showed the cellular viability results upon application of the enzyme at these different concentrations. A porous structure was observed as a result of the removal of the Alg from the matrix, which resulted in enhanced cellular viability within the constructs. When the effects of different enzyme concentrations are compared, it is seen that the increase rate in cell proliferation is higher when the enzyme is applied at lower rates.

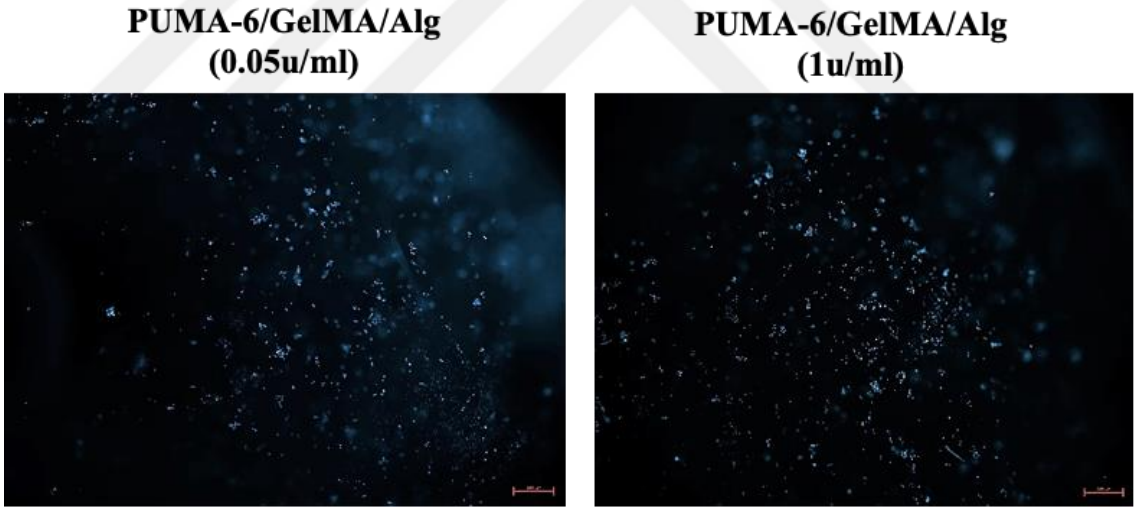

Figure 4.28 DAPI staining of the cells within PUMA-6/GelMA/Alg bioink (Day 7, 4x)

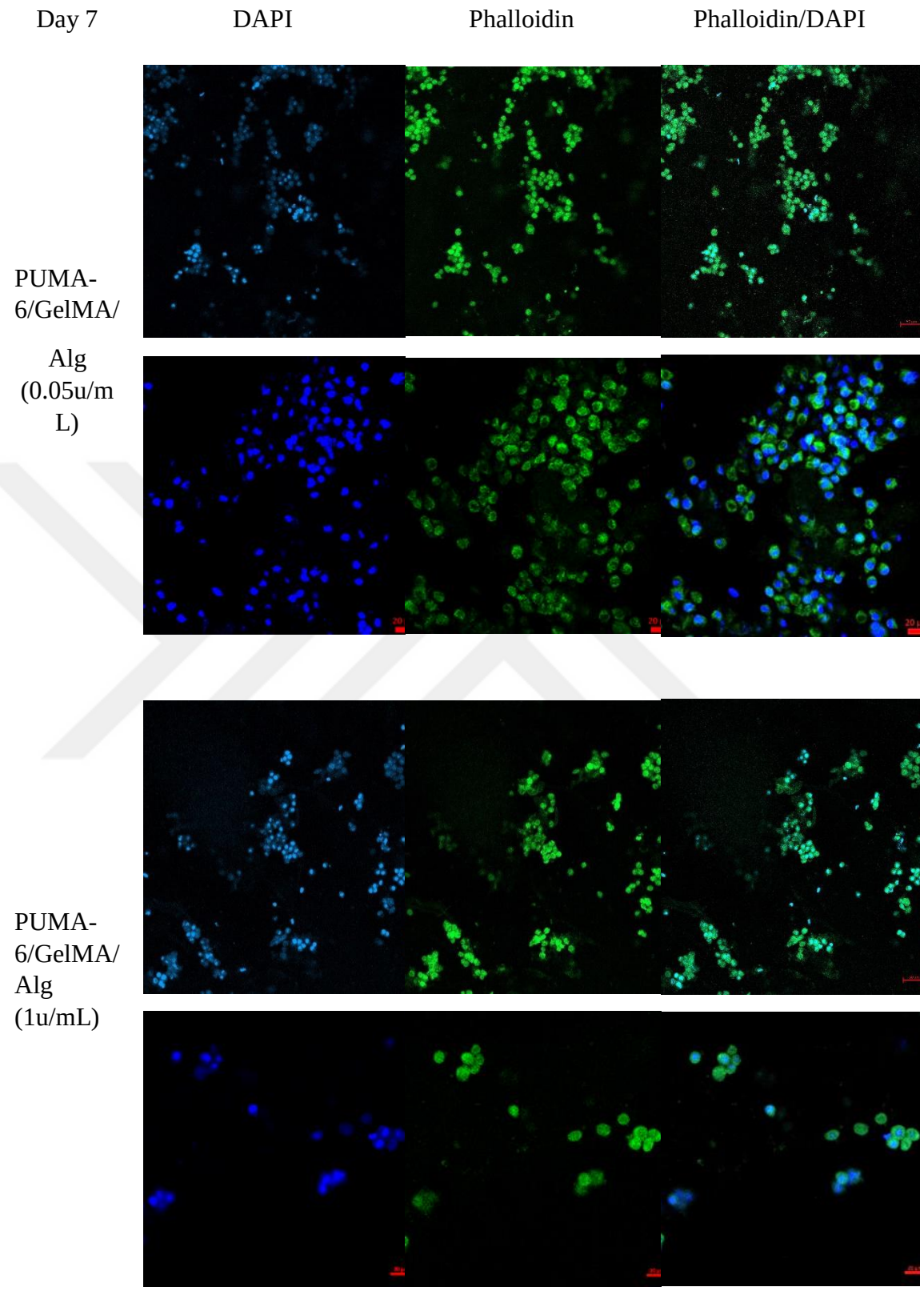

Figure 4.29 Confocal Laser Scanning Microscopy imaging of PUMA-6/GelMA/Alg bioink containing C2C12 cells on Day 7. 5x and 20x magnification. Scale bar = 50µm and 20µm. Channels: Phalloidin (green) and DAPI (blue)

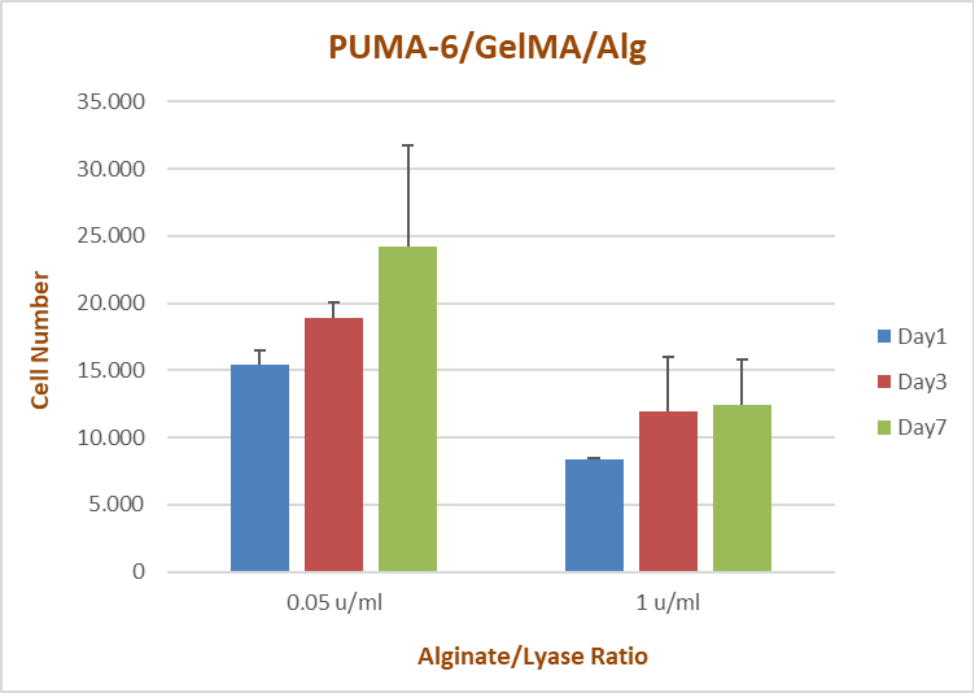

Figure 4.30 Assessment of cell viability with Alamar Blue assay within PUMA-6/GelMA/Alg bioink during culture

SEM images of the 3 different bioinks that were developed 1) PUMA-6, 2) PUMA-6/GelMA, 3) PUMA-6/GelMA/Alg are given in **Figure 4.31**. Insufficient cell proliferation in cell culture studies carried out with PUMA-6 bioinks is also evident in SEM analyzes by the smaller size of the pores. In the images obtained with PUMA-6/GelMA, porosity is seen much more than PUMA-6. In the studies conducted by adding alg, an increase in the size of the pores was observed as the alg were removed from the environment with the lyase enzyme in order to increase cell viability and ensure its spread. This shows that the alg/lyase activity was successful.

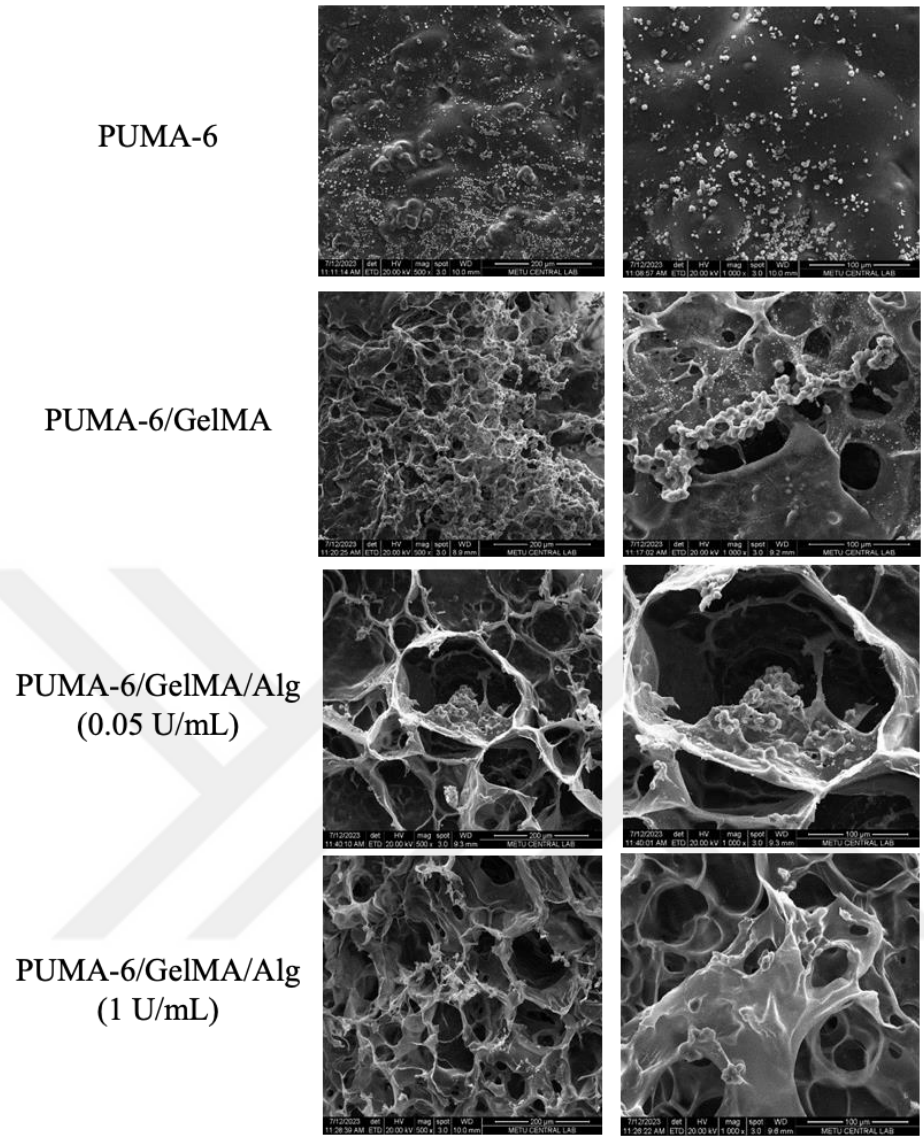

Figure 4.31 SEM images of cell-laden PU-based bioinks and blends (Scale bar: 200μm and 100μm)

In sum, 3D printing was possible, UV light exposure was reduced, and cell viability could be demonstrated by PUMA-6/GelMA/Alg bioink.

5. CONCLUSION

Skeletal muscle constitutes approximately half of the whole-body mass. It consists of striatedly arranged, parallel aligned, densely packed bundles of myofibers. Skeletal muscle tissue has the capacity of self-renewal upon injury. However, this regeneration capacity is insufficient and functional regeneration cannot occur in muscle losses that occur in a volume above a critical value. In such cases, there is a need for the use of conjugates that can be used in substitution of muscle function and there is a need for biomaterials to supportthe function of functional skeletal muscle.

Approaches to generate skeletal muscle-like structures in the laboratory using tissue engineering technique have the potential to solve the long-term problem of muscle loss in the clinic. 3D printing techniques are being utilized in this direction. 3D printing is the general term for modern technological production processes that enable the layer-by-layer formation of 3D items from data obtained from computer-controlled designs. The resulting 3D matrices require a certain degree of stability, but also appropriate biocompatibility to allow for cell adhesion, proliferation and differentiation. Today, with the use of cell-containing biomaterials, also called as "bioinks", it has become possible to produce living, functional tissues and organs in a laboratory environment with the 3D printing method. To create these structures, a solution of biomaterials in hydrogel form or a mixture of several biomaterials is used, which encapsulates the desired cell types. This bioink can be crosslinked or stabilized during or immediately after bioprinting to create the final shape, structure and architecture of the designed structure. The scarcity of biomaterials used as bioinks in the literature indicates the intensification of studies in this field.

Polyurethanes (PU) are among the most important polymers used as biomaterials. In the literature, the preparation of PUs as bioinks and their use in nerve tissue engineering have been mentioned, but no study has been found on skeletal muscle tissue engineering. Based on this gap in the literature, it was aimed to develop a bioink material based on PU and to create biocompatible, mechanically robust tissue structures in hydrogel

structure that can be produced by 3D bioprinting.

This thesis discusses the development of materials that can be used as novel bioink materials with desired mechanical properties as well as structural stability which is highly required in the literature. Light-curable polyurethane-based hydrogel structures were developed. Following that, 3D print optimization were carried out in order to create a structure suited for 3D bioprinting. As a result, three different compositions (1) PUMA-6, (2) PUMA-6/GelMA, and (3) PUMA-6/GelMA/Alg were used, which are suitable for 3D printing as light-curable, polyurethane-based bioink matrix.

REFERENCES

Ahmed, E. M. (2015a). Hydrogel: Preparation, characterization, and applications: A review. *Journal of Advanced Research*, *6*(2), 105–121. https://doi.org/10.1016/j.jare.2013.07.006

Ahmed, E. M. (2015b). Hydrogel: Preparation, characterization, and applications: A review. *Journal of Advanced Research*, *6*(2), 105–121. https://doi.org/10.1016/j.jare.2013.07.006

Aimar, A., Palermo, A., & Innocenti, B. (2019). The Role of 3D Printing in Medical Applications: A State of the Art. *Journal of Healthcare Engineering*, *2019*, 1–10. https://doi.org/10.1155/2019/5340616

AKKUŞ, H., GÜNAYDIN, B., & USTUNDAG, C. (2020). DOKU MÜHENDİSLİĞİNDE 3 BOYUTLU BİYO-BASKI İÇİN BİYOFONKSİYONEL MÜREKKEPLER. *International Journal of 3D Printing Technologies and Digital Industry*. https://doi.org/10.46519/ij3dptdi.795922

Caló, E., & Khutoryanskiy, V. V. (2015). Biomedical applications of hydrogels: A review of patents and commercial products. *European Polymer Journal*, *65*, 252–267. https://doi.org/10.1016/j.eurpolymj.2014.11.024

CAN, N., & ERSOY, M. S. (2014). Nanofiber Structured Polymeric Tissue Scaffolds. *Tekstil ve Mühendis*, 38–50. https://doi.org/10.7216/130075992014219505

Cascone, M. G., Barbani, N., P.Giusti, C. C., Ciardelli, G., & Lazzeri, L. (2001). Bioartificial polymeric materials based on polysaccharides. *Journal of Biomaterials Science, Polymer Edition*, *12*(3), 267–281. https://doi.org/10.1163/156856201750180807

Cezar, C. A., & Mooney, D. J. (2015). Biomaterial-based delivery for skeletal muscle repair. *Advanced Drug Delivery Reviews*, *84*, 188–197. https://doi.org/10.1016/j.addr.2014.09.008

Choi, Y. J., Kim, T. G., Jeong, J., Yi, H. G., Park, J. W., Hwang, W., & Cho, D. W. (2016). 3D Cell Printing of Functional Skeletal Muscle Constructs Using Skeletal Muscle-Derived Bioink. *Advanced Healthcare Materials*, *5*(20), 2636–2645. https://doi.org/10.1002/adhm.201600483

Cooper GM. (2000). Actin, Myosin, and Cell Movement. In *A Molecular Approach* (2nd ed.). Sinauer Associates.

Dawood, A., Marti, B. M., Sauret-Jackson, V., & Darwood, A. (2015). 3D printing in dentistry. *British Dental Journal*, *219*(11), 521–529. https://doi.org/10.1038/sj.bdj.2015.914

Derby, B. (2012). Printing and Prototyping of Tissues and Scaffolds. *Science*, *338*(6109), 921–926. https://doi.org/10.1126/science.1226340

Ergene, E., Yagci, B. S., Gokyer, S., Eyidogan, A., Aksoy, E. A., & Yilgor Huri, P. (2019a). A novel polyurethane-based biodegradable elastomer as a promising

material for skeletal muscle tissue engineering. *Biomedical Materials (Bristol)*, *14*(2). https://doi.org/10.1088/1748-605X/ab007a

Ergene, E., Yagci, B. S., Gokyer, S., Eyidogan, A., Aksoy, E. A., & Yilgor Huri, P. (2019b). A novel polyurethane-based biodegradable elastomer as a promising material for skeletal muscle tissue engineering. *Biomedical Materials*, *14*(2), 025014. https://doi.org/10.1088/1748-605X/ab007a

Fan, Y., Maley, M., Beilharz, M., & Grounds, M. (1996). Rapid death of injected myoblasts in myoblast transfer therapy. *Muscle & Nerve*, *19*(7), 853–860. https://doi.org/10.1002/(SICI)1097-4598(199607)19:7<853::AID-MUS7>3.0.CO;2-8

Ferreira, N. N., Ferreira, L. M. B., Cardoso, V. M. O., Boni, F. I., Souza, A. L. R., & Gremião, M. P. D. (2018). Recent advances in smart hydrogels for biomedical applications: From self-assembly to functional approaches. *European Polymer Journal*, *99*, 117–133. https://doi.org/10.1016/j.eurpolymj.2017.12.004

Friedmann-Morvinski, D., & Verma, I. M. (2014). Dedifferentiation and reprogramming: origins of cancer stem cells. *EMBO Reports*, *15*(3), 244–253. https://doi.org/10.1002/embr.201338254

Frontera, W. R., & Ochala, J. (2015). Skeletal Muscle: A Brief Review of Structure and Function. *Calcified Tissue International*, *96*(3), 183–195. https://doi.org/10.1007/s00223-014-9915-y

García-Lizarribar, A., Fernández-Garibay, X., Velasco-Mallorquí, F., Castaño, A. G., Samitier, J., & Ramon-Azcon, J. (2018). Composite Biomaterials as Long-Lasting Scaffolds for 3D Bioprinting of Highly Aligned Muscle Tissue. *Macromolecular Bioscience*, *18*(10), e1800167. https://doi.org/10.1002/mabi.201800167

Gokyer, S., Yilgor, E., Yilgor, I., Berber, E., Vrana, E., Orhan, K., Monsef, Y. A., Guvener, O., Zinnuroglu, M., Oto, C., & Yilgor Huri, P. (2021). 3D Printed Biodegradable Polyurethaneurea Elastomer Recapitulates Skeletal Muscle Structure and Function. *ACS Biomaterials Science & Engineering*, *7*(11), 5189–5205. https://doi.org/10.1021/acsbiomaterials.1c00703

Gungor-Ozkerim, P. S., Inci, I., Zhang, Y. S., Khademhosseini, A., & Dokmeci, M. R. (2018). Bioinks for 3D bioprinting: an overview. *Biomaterials Science*, *6*(5), 915–946. https://doi.org/10.1039/C7BM00765E

H. J. Chen, M. G. (2012). *A Roadmap from Idea to Implementation: 3D Printing for Pre-Surgical Application* (1st ed.).

Han, F., Wang, J., Ding, L., Hu, Y., Li, W., Yuan, Z., Guo, Q., Zhu, C., Yu, L., Wang, H., Zhao, Z., Jia, L., Li, J., Yu, Y., Zhang, W., Chu, G., Chen, S., & Li, B. (2020). Tissue Engineering and Regenerative Medicine: Achievements, Future, and Sustainability in Asia. *Frontiers in Bioengineering and Biotechnology*, *8*, 83. https://doi.org/10.3389/FBIOE.2020.00083/BIBTEX

Ho, L., & Hsu, S.-H. (2018). Cell reprogramming by 3D bioprinting of human fibroblasts in polyurethane hydrogel for fabrication of neural-like constructs. *Acta Biomaterialia*, *70*, 57–70. https://doi.org/10.1016/j.actbio.2018.01.044

Hockaday, L. A., Kang, K. H., Colangelo, N. W., Cheung, P. Y. C., Duan, B., Malone, E., Wu, J., Girardi, L. N., Bonassar, L. J., Lipson, H., Chu, C. C., & Butcher, J. T. (2012). Rapid 3D printing of anatomically accurate and mechanically heterogeneous aortic valve hydrogel scaffolds. *Biofabrication*, *4*(3), 035005. https://doi.org/10.1088/1758-5082/4/3/035005

Hölzl, K., Lin, S., Tytgat, L., Van Vlierberghe, S., Gu, L., & Ovsianikov, A. (2016). Bioink properties before, during and after 3D bioprinting. *Biofabrication*, *8*(3), 032002. https://doi.org/10.1088/1758-5090/8/3/032002

Hospodiuk, M., Dey, M., Sosnoski, D., & Ozbolat, I. T. (2017). The bioink: A comprehensive review on bioprintable materials. *Biotechnology Advances*, *35*(2), 217–239. https://doi.org/10.1016/j.biotechadv.2016.12.006

Huard, J., Li, Y., & Fu, F. H. (2002). Muscle injuries and repair: current trends in research. *The Journal of Bone and Joint Surgery. American Volume*, *84*(5), 822–832.

Ikada, Y. (2006). Challenges in tissue engineering. *Journal of The Royal Society Interface*, *3*(10), 589–601. https://doi.org/10.1098/RSIF.2006.0124

Khademhosseini, A., & Langer, R. (2016). A decade of progress in tissue engineering. *Nature Protocols*, *11*(10), 1775–1781. https://doi.org/10.1038/nprot.2016.123

Kim, J. H., Seol, Y.-J., Ko, I. K., Kang, H.-W., Lee, Y. K., Yoo, J. J., Atala, A., & Lee, S. J. (2018). 3D Bioprinted Human Skeletal Muscle Constructs for Muscle Function Restoration. *Scientific Reports*, *8*(1), 12307. https://doi.org/10.1038/s41598-018-29968-5

Koslen. (2020, November 15). *What is TPU material*. Https://Www.Tpupolymer.Com/What-Is-Tpu-Material_n7.

Kramschuster, A., & Turng, L.-S. (2013). Fabrication of Tissue Engineering Scaffolds. In *Handbook of Biopolymers and Biodegradable Plastics* (pp. 427–446). Elsevier. https://doi.org/10.1016/B978-1-4557-2834-3.00017-3

Ku, S. H., Lee, S. H., & Park, C. B. (2012). Synergic effects of nanofiber alignment and electroactivity on myoblast differentiation. *Biomaterials*, *33*(26), 6098–6104. https://doi.org/10.1016/j.biomaterials.2012.05.018

Langer, R. (2000). Tissue engineering. *Molecular Therapy : The Journal of the American Society of Gene Therapy*, *1*(1), 12–15. https://doi.org/10.1006/mthe.1999.0003

Langer, R., & Vacanti, J. P. (1993). Tissue Engineering. *Science*, *260*(5110), 920–926. https://doi.org/10.1126/science.8493529

Lee, V., Singh, G., Trasatti, J. P., Bjornsson, C., Xu, X., Tran, T. N., Yoo, S.-S., Dai, G., & Karande, P. (2014). Design and Fabrication of Human Skin by Three-Dimensional Bioprinting. *Tissue Engineering Part C: Methods*, *20*(6), 473–484. https://doi.org/10.1089/ten.tec.2013.0335

Lei, M., & Wang, X. (2016). Biodegradable Polymers and Stem Cells for Bioprinting. *Molecules*, *21*(5), 539. https://doi.org/10.3390/molecules21050539

Li, W. J., Mauck, R. L., Cooper, J. A., Yuan, X., & Tuan, R. S. (2007). Engineering controllable anisotropy in electrospun biodegradable nanofibrous scaffolds for

musculoskeletal tissue engineering. *Journal of Biomechanics*, *40*(8), 1686–1693. https://doi.org/10.1016/j.jbiomech.2006.09.004

Liao, H., & Zhou, G.-Q. (2009). Development and progress of engineering of skeletal muscle tissue. *Tissue Engineering. Part B, Reviews*, *15*(3), 319–331. https://doi.org/10.1089/ten.teb.2009.0092

Lloyd, A. W., Faragher, R. G. A., & Denyer, S. P. (2001). Ocular biomaterials and implants. *Biomaterials*, *22*(8), 769–785. https://doi.org/10.1016/S0142-9612(00)00237-4

Macaluso, F., & Myburgh, K. H. (2012). Current evidence that exercise can increase the number of adult stem cells. *Journal of Muscle Research and Cell Motility*, *33*(3–4), 187–198. https://doi.org/10.1007/s10974-012-9302-0

MacLean, S., Khan, W. S., Malik, A. A., Anand, S., & Snow, M. (2012). The potential of stem cells in the treatment of skeletal muscle injury and disease. In *Stem Cells International*. https://doi.org/10.1155/2012/282348

Malafaya, P. B., Silva, G. A., & Reis, R. L. (2007). Natural–origin polymers as carriers and scaffolds for biomolecules and cell delivery in tissue engineering applications. *Advanced Drug Delivery Reviews*, *59*(4–5), 207–233. https://doi.org/10.1016/j.addr.2007.03.012

Mannoor, M. S., Jiang, Z., James, T., Kong, Y. L., Malatesta, K. A., Soboyejo, W. O., Verma, N., Gracias, D. H., & McAlpine, M. C. (2013). 3D Printed Bionic Ears. *Nano Letters*, *13*(6), 2634–2639. https://doi.org/10.1021/nl4007744

McCullen, S. D., Ramaswamy, S., Clarke, L. I., & Gorga, R. E. (2009). Nanofibrous composites for tissue engineering applications. *WIREs Nanomedicine and Nanobiotechnology*, *1*(4), 369–390. https://doi.org/10.1002/wnan.39

Melchels, F. P. W., Domingos, M. A. N., Klein, T. J., Malda, J., Bartolo, P. J., & Hutmacher, D. W. (2012). Additive manufacturing of tissues and organs. *Progress in Polymer Science*, *37*(8), 1079–1104. https://doi.org/10.1016/j.progpolymsci.2011.11.007

Merceron, T. K., Burt, M., Seol, Y. J., Kang, H. W., Lee, S. J., Yoo, J. J., & Atala, A. (2015). A 3D bioprinted complex structure for engineering the muscle-tendon unit. *Biofabrication*, *7*(3). https://doi.org/10.1088/1758-5090/7/3/035003

Michael Walden. (2022, September 21). *Skeletal Muscle Structure*. Https://Www.Teachpe.Com/Anatomy-Physiology/Structure-of-Skeletal-Muscle.

Miyazaki, T., & Hotta, Y. (2011). CAD/CAM systems available for the fabrication of crown and bridge restorations. *Australian Dental Journal*, *56*, 97–106. https://doi.org/10.1111/j.1834-7819.2010.01300.x

Moysidou, C. M., Barberio, C., & Owens, R. M. (2021). Advances in Engineering Human Tissue Models. *Frontiers in Bioengineering and Biotechnology*, *8*, 1566. https://doi.org/10.3389/FBIOE.2020.620962/BIBTEX

Muhamad, I. I., Selvakumaran, S., & Lazim, N. A. (2014). Designing Polymeric Nanoparticles for Targeted Drug Delivery System. In Professor Alexander Seifalian, Achala de Mel, & Deepak M. Kalaskar (Eds.), *Nanomedicine*. One Central Press (OCP).

Murphy, S. V., & Atala, A. (2014a). 3D bioprinting of tissues and organs. In *Nature Biotechnology* (Vol. 32, Issue 8, pp. 773–785). Nature Publishing Group. https://doi.org/10.1038/nbt.2958

Murphy, S. V., & Atala, A. (2014b). 3D bioprinting of tissues and organs. In *Nature Biotechnology* (Vol. 32, Issue 8, pp. 773–785). Nature Publishing Group. https://doi.org/10.1038/nbt.2958

Pati, F., Ha, D.-H., Jang, J., Han, H. H., Rhie, J.-W., & Cho, D.-W. (2015). Biomimetic 3D tissue printing for soft tissue regeneration. *Biomaterials*, *62*, 164–175. https://doi.org/10.1016/j.biomaterials.2015.05.043

Peppas, N. (2000). Hydrogels in pharmaceutical formulations. *European Journal of Pharmaceutics and Biopharmaceutics*, *50*(1), 27–46. https://doi.org/10.1016/S0939-6411(00)00090-4

Puschmann, T. B., Zandén, C., De Pablo, Y., Kirchhoff, F., Pekna, M., Liu, J., & Pekny, M. (2013). Bioactive 3D cell culture system minimizes cellular stress and maintains the in vivo-like morphological complexity of astroglial cells. *Glia*, *61*(3), 432–440. https://doi.org/10.1002/glia.22446

Qazi, T. H., Mooney, D. J., Pumberger, M., Geißler, S., & Duda, G. N. (2015). Biomaterials based strategies for skeletal muscle tissue engineering : Existing technologies and future trends. *Biomaterials*, *53*, 502–521. https://doi.org/10.1016/j.biomaterials.2015.02.110

Quintero, A. J., Wright, V. J., Fu, F. H., & Huard, J. (2009). Stem Cells for the Treatment of Skeletal Muscle Injury. *Clinics in Sports Medicine*, *28*(1), 1–11. https://doi.org/10.1016/j.csm.2008.08.009

Radhakrishnan, J., Krishnan, U. M., & Sethuraman, S. (n.d.). Hydrogel based injectable scaffolds for cardiac tissue regeneration. *Biotechnology Advances*, *32*(2), 449–461. https://doi.org/10.1016/j.biotechadv.2013.12.010

Rivas, D. A., & Fielding, R. A. (2013). Skeletal Muscle. In *Encyclopedia of Human Nutrition* (pp. 193–199). Elsevier. https://doi.org/10.1016/B978-0-12-375083-9.00188-4

S. Hikida, R. (2011). Aging Changes in Satellite Cells and Their Functions. *Current Aging Sciencee*, *4*(3), 279–297. https://doi.org/10.2174/1874609811104030279

Satyanarayana, B., & Prakash, K. J. (2015). Component Replication Using 3D Printing Technology. *Procedia Materials Science*, *10*, 263–269. https://doi.org/10.1016/j.mspro.2015.06.049

Schaefer, B., Beier, J. P., & Ruhl, T. (2020). Mesenchymal Stem Cells and the Generation of Neomuscle Tissue. *Surgical Technology International*, *36*, 41–47.

Shafiee, A., & Atala, A. (2017). Tissue Engineering: Toward a New Era of Medicine. *Https://Doi.Org/10.1146/Annurev-Med-102715-092331*, *68*, 29–40. https://doi.org/10.1146/ANNUREV-MED-102715-092331

Skardal, A., Zhang, J., & Prestwich, G. D. (2010). Bioprinting vessel-like constructs using hyaluronan hydrogels crosslinked with tetrahedral polyethylene glycol tetracrylates. *Biomaterials*, *31*(24), 6173–6181. https://doi.org/10.1016/j.biomaterials.2010.04.045

Strub, J. R., Rekow, E. D., & Witkowski, S. (2006). Computer-aided design and fabrication of dental restorations. *The Journal of the American Dental Association*, *137*(9), 1289–1296. https://doi.org/10.14219/jada.archive.2006.0389

Thoma, C. R., Zimmermann, M., Agarkova, I., Kelm, J. M., & Krek, W. (2014). 3D cell culture systems modeling tumor growth determinants in cancer target discovery. In *Advanced Drug Delivery Reviews* (Vols. 69–70, pp. 29–41). Elsevier. https://doi.org/10.1016/j.addr.2014.03.001

Turner, N. J., & Badylak, S. F. (2012). Regeneration of skeletal muscle. *Cell and Tissue Research*, *347*(3), 759–774. https://doi.org/10.1007/s00441-011-1185-7

Tuzlakoglu, K., Bolgen, N., Salgado, A. J., Gomes, M. E., Piskin, E., & Reis, R. L. (2005). Nano- and micro-fiber combined scaffolds: A new architecture for bone tissue engineering. *Journal of Materials Science: Materials in Medicine*, *16*(12), 1099–1104. https://doi.org/10.1007/s10856-005-4713-8

Ullah, F., Othman, M. B. H., Javed, F., Ahmad, Z., & Akil, H. Md. (2015). Classification, processing and application of hydrogels: A review. *Materials Science and Engineering: C*, *57*, 414–433. https://doi.org/10.1016/j.msec.2015.07.053

ULUSOY, A., & DİKMEN, N. (2020). Hidrojellerin Tıpta Uygulamaları. *Arşiv Kaynak Tarama Dergisi*, *29*(2), 129–137. https://doi.org/10.17827/aktd.603432

Vannozzi, L., Ricotti, L., Santaniello, T., Terencio, T., Oropesa-Nunez, R., Canale, C., Borghi, F., Menciassi, A., Lenardi, C., & Gerges, I. (2017). 3D porous polyurethanes featured by different mechanical properties: Characterization and interaction with skeletal muscle cells. *Journal of the Mechanical Behavior of Biomedical Materials*, *75*, 147–159. https://doi.org/10.1016/j.jmbbm.2017.07.018

Vijayavenkataraman, S., Yan, W.-C., Lu, W. F., Wang, C.-H., & Fuh, J. Y. H. (2018). 3D bioprinting of tissues and organs for regenerative medicine. *Advanced Drug Delivery Reviews*, *132*, 296–332. https://doi.org/10.1016/j.addr.2018.07.004

Wang, W., Narain, R., & Zeng, H. (2020). Hydrogels. In *Polymer Science and Nanotechnology* (pp. 203–244). Elsevier. https://doi.org/10.1016/B978-0-12-816806-6.00010-8

Winkler, T., von Roth, P., Matziolis, G., Schumann, M. R., Hahn, S., Strube, P., Stoltenburg-Didinger, G., Perka, C., Duda, G. N., & Tohtz, S. V. (2011). Time course of skeletal muscle regeneration after severe trauma. *Acta Orthopaedica*, *82*(1), 102–111. https://doi.org/10.3109/17453674.2010.539498

WICHTERLE, O., & LÍM, D. (1960). Hydrophilic Gels for Biological Use. *Nature*, *185*(4706), 117–118. https://doi.org/10.1038/185117a0

Wolfe, R. R. (2006). The underappreciated role of muscle in health and disease1–3. *The American Journal of Clinical Nutrition*, *84*(3), 475–482. https://doi.org/10.1093/ajcn/84.3.475

Xia, Z., Jin, S., & Ye, K. (2018). Tissue and Organ 3D Bioprinting. *SLAS Technology*, *23*(4), 301–314. https://doi.org/10.1177/2472630318760515

XU, T., GREGORY, C., MOLNAR, P., CUI, X., JALOTA, S., BHADURI, S., & BOLAND, T. (2006). Viability and electrophysiology of neural cell structures

generated by the inkjet printing method. *Biomaterials*. https://doi.org/10.1016/j.biomaterials.2006.01.048

Xu, T., Olson, J., Zhao, W., Atala, A., Zhu, J.-M., & Yoo, J. J. (2008). Characterization of Cell Constructs Generated With Inkjet Printing Technology Using In Vivo Magnetic Resonance Imaging. *Journal of Manufacturing Science and Engineering*, *130*(2). https://doi.org/10.1115/1.2902857

Yilgör, I., Yilgör, E., & Wilkes, G. L. (2015). Critical parameters in designing segmented polyurethanes and their effect on morphology and properties: A comprehensive review. *Polymer*, *58*, A1–A36. https://doi.org/https://doi.org/10.1016/j.polymer.2014.12.014

Yin Yu, & Ozbolat, I. T. (2014). Tissue strands as “bioink” for scale-up organ printing. *2014 36th Annual International Conference of the IEEE Engineering in Medicine and Biology Society*, 1428–1431. https://doi.org/10.1109/EMBC.2014.6943868

Zhu, W., Ma, X., Gou, M., Mei, D., Zhang, K., & Chen, S. (2016). 3D printing of functional biomaterials for tissue engineering. *Current Opinion in Biotechnology*, *40*, 103–112. https://doi.org/10.1016/j.copbio.2016.03.014

APPENDICES

APPENDIX 1 Calibration curve of C2C12 (CRL-1772, ATCC) cells for Alamar Blue Assay

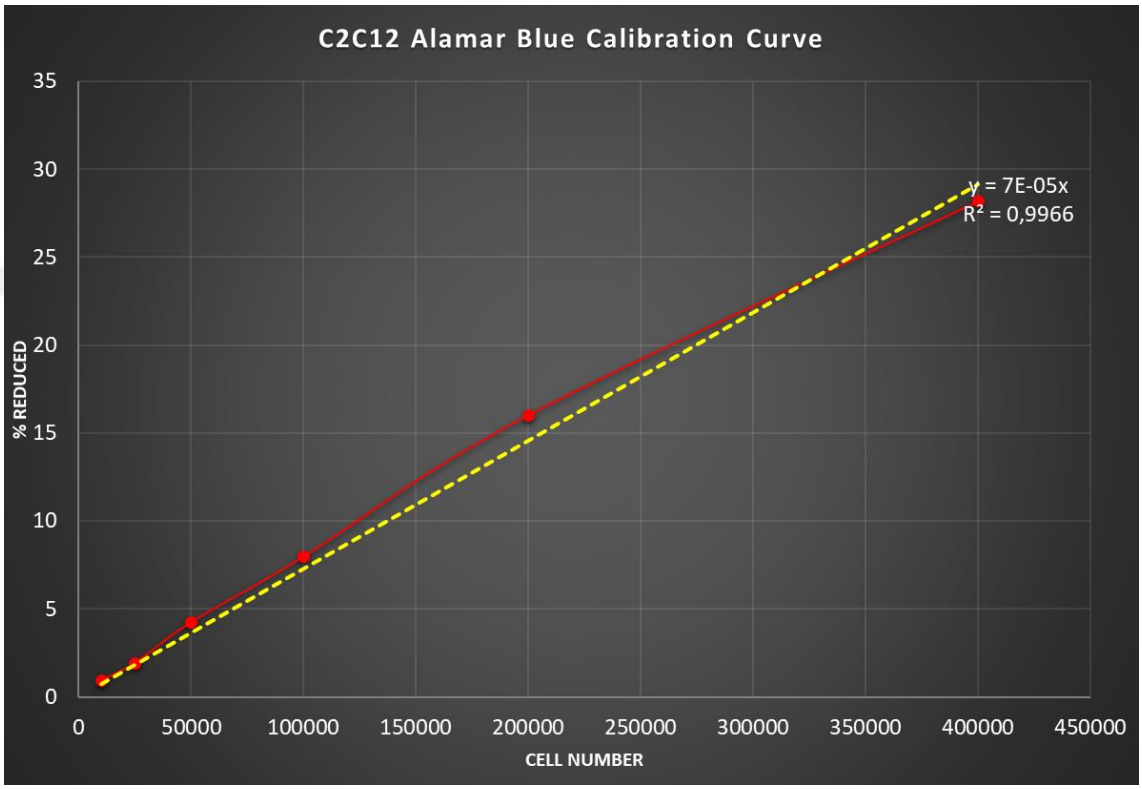

APPENDIX 2 Calibration curve of L929 cells for Alamar Blue Assay